Australian Government
Department of Defence
Defence Science and
Technology Organisation

DSTO

Wind Tunnel Simulations of the Mock Urban Setting Test - Experimental Procedures and Data Analysis

Ralph Gailis

DSTO-TR-1532

Australian Government
Department of Defence
Defence Science and
Technology Organisation

Wind Tunnel Simulations of the Mock Urban Setting Test—Experimental Procedures and Data Analysis

Ralph Gailis

CBRN Defence Centre
Platforms Sciences Laboratory

DSTO–TR–1532

ABSTRACT

The MUST experiment was a large outdoor field study in atmospheric dispersion, attempting to simulate an urban boundary layer by the construction of a regular array of shipping containers. The current report gives details of a wind tunnel dispersion study of the MUST array, aimed at bridging some of the gaps between laboratory and full-scale outdoor trials. The experimental setup and wind tunnel instrumentation are discussed in detail, the measurements made together with the organisation of the dataset is fully described, and a comprehensive description of the data analysis techniques is given. Emphasis is placed on the scaling arguments used to compare data between a wind tunnel and full-scale study, and on methods of uncertainty analysis to provide a rigorous underpinning to the dataset. The report serves as a complete documentation for users of the MUST wind tunnel simulation dataset, which can be obtained by contacting the author.

Published by

DSTO Platforms Sciences Laboratory
506 Lorimer St,
Fishermans Bend, Victoria, Australia 3207

Telephone: *(03) 9626 7000*
Facsimile: *(03) 9626 7999*

AR No. 013–153
July, 2004

APPROVED FOR PUBLIC RELEASE

Wind Tunnel Simulations of the Mock Urban Setting Test—Experimental Procedures and Data Analysis

EXECUTIVE SUMMARY

Turbulent dispersion of contaminants in the atmosphere has a diverse range of interest and applications, but is only considered to be understood with confidence in settings involving level, unobstructed and fairly simple terrain, such as a rural environment. The study of dispersion within a far more complex urban environment has been receiving increasing interest over the past decade or two. As a consequence, numerous studies of dispersion within large idealised and regular obstacle arrays are beginning to appear in the literature. It is such a regime that seems to be the least understood, and most relevant to the study of atmospheric processes within urban areas. With a better understanding of dispersion on these scales, it is expected that generalisations can then be made to the far more random and complex realistic urban landscapes.

Many of the investigations on idealised array geometries have involved wind tunnel, water channel or small scale field trials. Current urban dispersion models tend to be constructed on the basis of these empirical results. It would seem important to provide some kind of comparison and validation of experiments performed at different scales and using different apparatus or in different conditions. This report documents experiments in a wind tunnel to simulate a large scale field trial of tracer dispersion, recently held at US Army Dugway Proving Ground, Utah. The field trial involved the study of dispersion within a regular array of large shipping containers (height 2.54 m, width 2.42 m and length 12.18 m), and was known as the Mock Urban Setting Test (MUST). Numerous releases of propylene, both continuous and puff, were performed within the array, to yield a comprehensive dataset of concentration time series, along with extensive supporting meteorological data. Many aspects of the field trials were simulated in the Monash University large environmental wind tunnel, at a scale of 1:50. Some of the issues investigated included the effects of different atmospheric stratification (particularly stable versus neutral stratification), a range of wind directions and release points, puff versus continuous releases, and supporting detailed wind velocity profiles.

The current report serves as the comprehensive documentation for the wind tunnel experiments. It describes the detailed experimental setup, including instrumentation, physical model layout, tunnel flow conditioning and boundary layer development, and the measurements made. Continuous reference is made to the organisation of the dataset and the notation used, in the hope of efficiently guiding users of the data. (The CD containing all the data can be obtained by contacting the author.) The methodology of the data analysis is also discussed in great detail, with particular emphasis on the appraisal of uncertainties in the measurements, and the construction of a logical framework to propagate these uncertainties through the various data reduction stages to the final reported experimental results. In this way, the author has attempted to provide a rigorous and high quality dataset, useful for a diverse range of applications, including inter-comparison with other datasets, fundamental studies of the mechanisms of plume dispersion within obstacle arrays, and validation of actual urban dispersion models.

With the experimental details and data analysis thoroughly documented in this report, future papers will further discuss detailed results and broader scientific interpretations of the data, including comparisons with the full-scale field trial, and another study of the MUST array at 1:200 scale in a water channel.

Author

Ralph Gailis
Chemical Biological Radiological and Nuclear Defence Centre

Ralph Gailis completed his undergraduate studies in physics and mathematics (Honours) at the University of Melbourne in 1992. He went on to do a Ph.D. on the topic of "Plasma Physics in the Early Universe" in the School of Physics, University of Melbourne from 1993–1996. 1997–1998 saw him continue on in the same department as a postdoctoral research fellow, until his recruitment in the Combatant Protection and Nutrition Branch at DSTO in 1999. Research interests at the University of Melbourne included statistical mechanics, general relativity, cosmology and plasma physics.

Since working at DSTO, Ralph has developed a programme on hazard assessment of chemical, biological and radiological weapons. The main focus of scientific research in this area has been in atmospheric dispersion modelling and turbulence theory. This has involved some challenging theoretical work, which has always been Ralph's forte, but also opened up a large new world of experimental science in wind tunnel and water channel simulations. The work has also involved operational support to provide the ADF with current state-of-the-art CBRN hazard prediction models, which have been used for a number of high profile events.

Ralph spent over a year in 2002–2003 working at DRDC (Suffield), Alberta, Canada under a Defence Science Fellowship, greatly extending his knowledge on the science behind CBR hazard assessment and dispersion modelling. He has also served the last five years as National Leader, TTCP CBD Group Technical Panel 9 (Hazard Assessment). These invaluable international interactions have helped the development of the DSTO programme in this area immensely.

Contents

Appendices

Figures

Tables

Notation

$\langle\,\rangle$	A generic averaging process (usually over an ensemble)
$\hat{X}$	Statistical estimator of a parameter X
a	Source flow rate calibration constant, $a = 5.67 \times 10^{-5}$
A	Mean of a raw a/d level time series
A_i	Individual raw time series sample expressed as an a/d level
A_t	Mean of a baseline corrected a/d level time series
b	Source flow rate calibration constant, $b = 0.514$
B	Time series baseline correction value (in a/d levels)
B_r	Buoyancy parameter—ratio of buoyancy to free-stream momentum flux
c_b	Baseline correction uncertainty sensitivity factor
c_c	Concentration calibration uncertainty sensitivity factor
c_l	Reference length scale uncertainty sensitivity factor
c_r	Source flow rate uncertainty sensitivity factor
c_s	Stochastic variability uncertainty sensitivity factor
c_i	Sensitivity factor of uncertainty component i
c_u	Reference wind speed uncertainty sensitivity factor
C	Generic concentration (usually expressed as volume fraction)
$\overline{C}$	Mean concentration
$\overline{C^2}$	Mean square concentration
C_0	Maximum plume centreline concentration
d	Diameter of the source at the point of release
d_s	Displacement height of the vertical mean velocity profile
F_r	Mass flow rate ratio (discharge to free-stream flow)
g	Acceleration due to gravity
H	Height of the array obstacles (= 48 mm in model scale)
i_c	Fluctuation intensity of concentration
i_u	Turbulence intensity in the direction of mean wind
K	Dimensionless concentration
k_c	Kurtosis of concentration
k_i	Channel i linear calibration constant for concentration vs. voltage
L	Characteristic length scale of a model
M_r	Momentum parameter—ratio of plume to free-stream momentum flux
n	Number of items in a generic ensemble
N	Number of samples in a time series

Q	Source flow rate
R	Source flow rate gauge reading (arbitrary units)
R_b	Bulk Richardson number
R_c	Critical Richardson number
r_b	Semi-range of baseline correction uncertainty distribution
r_l	Semi-range of reference length scale uncertainty distribution
r_r	Semi-range of source flow rate uncertainty distribution
r_u	Semi-range of reference wind speed uncertainty distribution
s_c	Skewness of concentration
T_0	Temperature measured at the surface
T_z	Temperature measured at height z
u	Mean wind speed in the direction of mean flow
u_*	Surface friction velocity
u_{50}	Mean wind speed at 50 m height (in full-scale)
u_b	Baseline correction standard uncertainty
u_c	Concentration calibration standard uncertainty
u_i	Standard uncertainty of component i
u_l	Reference length scale standard uncertainty
u_r	Source flow rate standard uncertainty
u_s	Intrinsic stochastic uncertainty, given at a 1-σ level
u_{si}	Intrinsic stochastic uncertainty determined for a particular channel i, in a set of repeated measurements
u_{tot}	Total standard uncertainty in a measurement
u_u	Reference wind speed standard uncertainty
v	Mean wind speed in the y-direction
v_a	a/d level to voltage conversion factor, $v_a = 10000/2048$
V_a	Volume fraction of air
V_g	Volume fraction of tracer gas
w	Mean vertical velocity (of air or effluent)
x	Spatial coordinate along the columns of the obstacle array
x_i	Generic variable denoting sample number i in a time series
y	Spatial coordinate along the rows of the obstacle array
y_i	Generic variable denoting a particular sample number i of a measured physical quantity Y
z	Vertical spatial coordinate ($z = 0$ is the surface)
z_0	Aerodynamic roughness length

z_c	Plume centroid position
$\Delta\rho$	Density difference of air and effluent $\rho_a - \rho_g$
Δu_s	Standard deviation in the collection of stochastic uncertainties for a group of channels
χ^2	Statistical goodness-of-fit parameter
κ	Von Karman's constant (assume $\kappa = 0.4$)
ρ_g	Density of effluent
ρ_a	Density of air
σ_A	Standard deviation of a/d level time series
σ_c	Standard deviation of instantaneous concentration
σ_K	Standard deviation of an ensemble of mean dimensionless concentration measurements
σ_u	Standard deviation of velocity in the direction of the mean wind
σ_Y	Overall experimental standard uncertainty for a physical quantity Y
σ_y	Lateral (horizontal) plume spread
σ_z	Vertical plume spread
σ_ϵ^2	Aggregate instrumental Type B uncertainty (variance) of a measured quantity
σ_τ^2	Intrinsic stochastic uncertainty (variance) of a measured quantity

1 Introduction

The turbulent dispersion of scalar quantities (such as contaminants) in the atmosphere lends itself to a diverse range of interest and applications. Although fairly well understood in open (or unobstructed), relatively flat terrain (see e.g. [1]), dispersion in an urban environment is considerably less well understood, mainly due to the great complexities introduced when a turbulent flow interacts with an almost limitless range in shape, size and configuration of obstacles. Older studies of dispersion around obstacles tended to focus more on the flow and short range dispersion around single and small groups of buildings. Excellent and comprehensive review articles have been given by Meroney [2] and Hosker [3], [4]. At the largest scales of interest, buildings tend to behave merely as roughness elements, and conventional dispersion theory (such as Gaussian plume models) is applicable, with some possible modifications on basic parameterisations. It is in the intermediate regime of scales, where the number of buildings in a group is large enough so that modelling of the effect of individual obstacles is prohibitive, that knowledge is most incomplete and new approaches need to be explored.

The most obvious way to understand some of the underlying physical processes at work in the intermediate regime of urban dispersion is to perform experimental investigations on geometrically simple arrays of obstacles. Some investigations in this area that have appeared in recent years, involving both field and wind tunnel studies, include the work of Davidson *et al.* [5], [6] and Macdonald *et al.* [7], [8]. These types of experiments often involve the investigation of dispersion within regular arrays of cubic or rectangular blocks, with the intent of simulating urban boundary layers of varying morphological characteristics and area densities. Although real urban landscapes are considerably more complex than the idealised, simple geometries considered in these studies, it is through such a comprehensive and controlled study of a wide range of idealised configurations that the underlying physical mechanisms of dispersion can be probed, and a quantitative picture of the important processes developed. Such physical simulation of atmospheric dispersion in an urban environment, coupled with the development of mathematical and computer models for the prediction of contaminant dispersion, has steadily been gaining more interest over the last decade. One example of such an empirical model to come out in the past few years is the UK Defence Science and Technology Laboratory UDM (Urban Dispersion Model) [9], [10]. There exist still relatively few experimental datasets, particularly outdoor experiments and trials in real urban areas, to serve as guidance in the development of more complex, physics-based models of urban dispersion, as well as in their validation. This is mainly due to the very high cost of outdoor dispersion and meteorological trials, and the even greater challenges encountered in terms of logistics and permitting, with performing trials in an urban area. Urban dispersion model parameterisations to date have generally relied on data obtained from wind tunnels or water channels, as well as some small scale outdoor trials. The need to validate existing computational models with realistic full-scale data, as well as to validate the wind tunnel datasets themselves, is becoming a pressing issue.

In an attempt to begin to bridge the gap between wind tunnel and full-scale experiments, a large field trial was recently held at US Army Dugway Proving Ground, Utah. This field trial, known as the Mock Urban Setting Test (MUST), consisted of a 10 by 12 regular array of 120 shipping containers, through which the dispersion of tracer gases

was measured [11], [12], [13], [14], [15]. The trial dataset also consists of an accompanying wealth of sonic and meteorological data to complement the concentration data of the tracer dispersion. The MUST experiment, which involved a fairly typical example of the arrays that have been studied in scaled models, provided an important opportunity to make comparisons with scaled laboratory experiments. In particular, two separate datasets have been obtained for comparison with the full-scale trials, one in a large wind tunnel at 1:50 scale (discussed in this report), and one in a water channel at 1:205 scale (yet to be published).

The simulation of a full-scale trial at a number of different scales has a variety of motivations, some alluded to above. Most importantly, features of the dispersion process that transcend the various scales can be studied, and an appreciation can be gained of how well the simplified and controlled environment of a wind tunnel or water channel can reproduce full-scale results. This will lead to an understanding of the validity and limitations of the scaled experiments as an aid to constructing algorithms for atmospheric dispersion models. The behaviour of the real atmosphere is extremely variable and often difficult to measure and characterise. Wind tunnels, on the other hand, provide strictly controlled experimental environments, where particular configurations of interest can be investigated in detail, thus being able to fill in data gaps inevitably encountered in a full-scale trial. Certain interesting configurations may just not become realised in a particular full-scale trial (for example a particular wind direction of interest). Because of the ability to tightly control parameters in a wind tunnel, more stationary conditions can be simulated, giving measurements and results based on more certain input conditions. This leads to better convergence of the statistics of time series measurements, or better stochastic stationarity. It also provides better defined boundary conditions when running computational models for validation or other purposes, which is of critical importance in complex calculations such as those undertaken in computational fluid dynamics (CFD) work.

The current report will describe in detail the work done at the large Environmental Wind Tunnel, housed in the Department of Mechanical Engineering at Monash University, Clayton, Australia. A detailed dispersion study was conducted on a 1:50 scale model of the MUST array, in both neutral and stable atmospheric stratification conditions, together with some supporting flow measurements (for some preliminary results, see [16]). This report will discuss the experimental design and procedure, as well as the data analysis approach, and will thus serve as the comprehensive documentation to the wind tunnel dataset of the MUST array. Future papers will make detailed comparisons with the MUST full-scale and water channel datasets, in an endeavour to further explore the issues arising with scaled model simulations.

The report will be organised as follows. A description of the wind tunnel facility and the experimental setup will be given in Section 2. This description includes a general overview of the wind tunnel facility, a description of the wind model used, a summary of measurements made, and a discussion of various scaling issues when comparing model with full-scale results. Section 3 will be concerned with a general description of the data analysis procedures undertaken. This involves an overview of the dataset, as found on the MUST Wind Tunnel Data CD, baseline corrections and calibration of time series, and general extraction of concentration statistics. In Section 4, a detailed exposition on the methods of uncertainty analysis used on the data will be given. Evaluation of the most important contributions to uncertainty will be thoroughly discussed. Finally, some

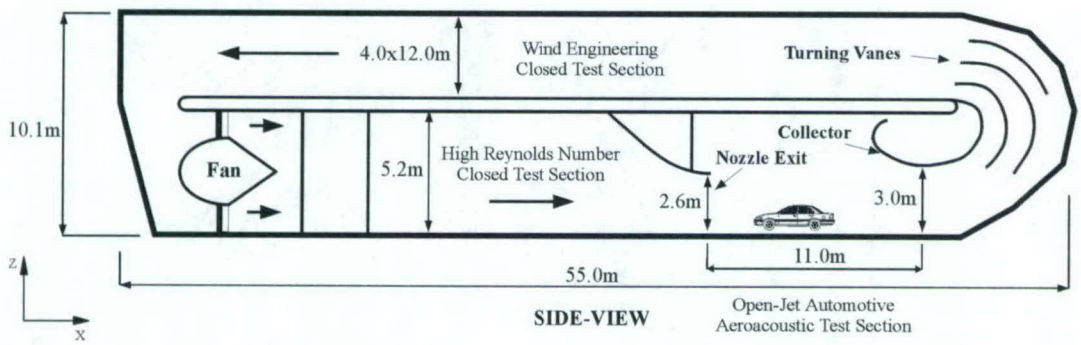

Figure 2.1: A schematic diagram of the Monash University wind tunnel facility

conclusions and further possible work are outlined in Section 5.

2 Experimental Details

2.1 Overview of the Wind Tunnel Facility

The 1.5 MW Boundary Layer Wind Tunnel in the Department of Mechanical Engineering, Monash University, Australia, is one of the largest of its kind in the world. The tunnel is managed by Prof. W. Melbourne, and the tunnel operator for the trials was H. Fricke. The full dimensions of the tunnel are 4 m high, 12 m wide, and 55 m in length. The actual length of the working section is about 10–12 m, with the remainder of the floor space devoted to heating elements for modelling convective flows, and other flow conditioning devices used to accelerate boundary layer development. The tunnel is of a continuously recirculating design, and the working space for the dispersion experiments was in the upper level. The model could be placed on a large turntable, and oriented in any direction relative to the incoming wind. See Figure 2.1 for a schematic diagram of the facility, and Figure 2.2 for a photo of the wind tunnel facility, showing the MUST obstacle array, flow conditioning trip boards (see Section 2.6) and window to the control room. Many more photos of the obstacle array and wind tunnel setup are included in the data CD, under the directory `docs/photos`.

2.2 The MUST Obstacle Array

The full-scale MUST array consisted of 12 rows by 10 columns of shipping containers, each with height 2.54 m, width 2.42 m and length 12.18 m. The wind tunnel scale for the model was 1:50. Figure 2.3 contains an idealised diagram of the array, showing all the containers with rows labelled A–L, and columns labelled 0–9 (other features of the diagram, including source release points and sampling locations are discussed below). Measurements are given in equivalent full-scale dimensions, with wind direction 0 being taken as running parallel to the vertical (North-South) axis in the figure (true North in the field was actually

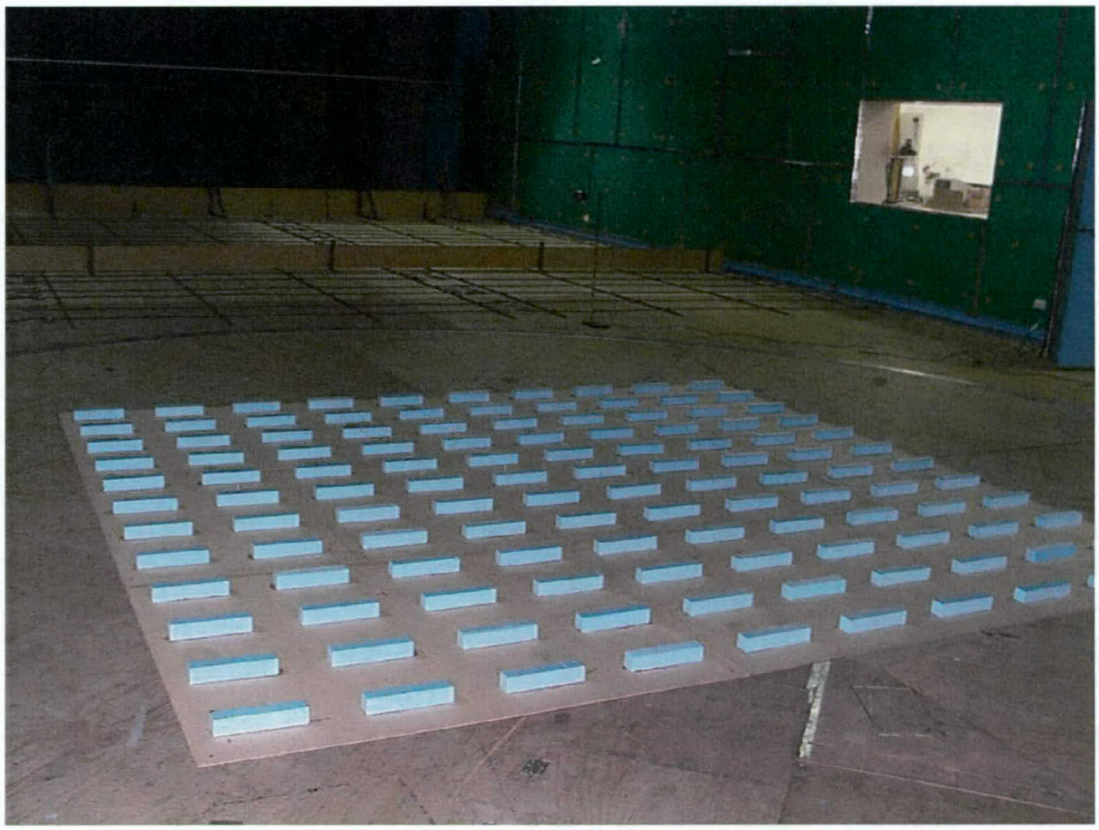

Figure 2.2: A photo of the Monash University wind tunnel facility, with the model of the MUST array, flow conditioning trip boards and a window to the control room all in view.

displaced about 30° clockwise of this line). We will adopt the convention in this report that the positive x-coordinate runs in the direction of North (obstacle column), and that the positive y-coordinate runs in the direction of West (obstacle row), in a usual right-handed system (similar to usual fluid flow conventions in the literature, where x runs in the direction of mean flow—see disucssion on wind directions later). The z-axis will point upwards, with $z = 0$ the surface. Due to the practical problems of positioning large shipping containers exactly, the spacing between the containers was not exactly the same for all rows and columns, but for the purposes of the wind tunnel model, the slight imperfections were averaged out, to give a regular spacing of 7.96 m in the lengthwise spacing of the containers, and 12.83 m in the span-wise spacing, as measured in equivalent full-scale lengths. A diagram indicating the container layout and dimensions is given in Figure 2.4. Some source release positions are also given in this diagram, which will be discussed in more detail in Section 2.7.

The MUST obstacle array model was positioned within the upper test section of the tunnel, directly centred on the large turntable in the middle of the tunnel. At the 1:50 scale used, the dimensions of the model obstacles are height 48 mm, width 48 mm and length 244 mm (note a slight discrepancy in the properly scaled height of the model obstacles, due to inaccurate information on the exact height of the full-scale shipping containers at the time of model construction). The obstacles were spaced by the average length $\langle w \rangle = 159$ mm in the span-wise direction and $\langle l \rangle = 257$ mm in the lengthwise direction.

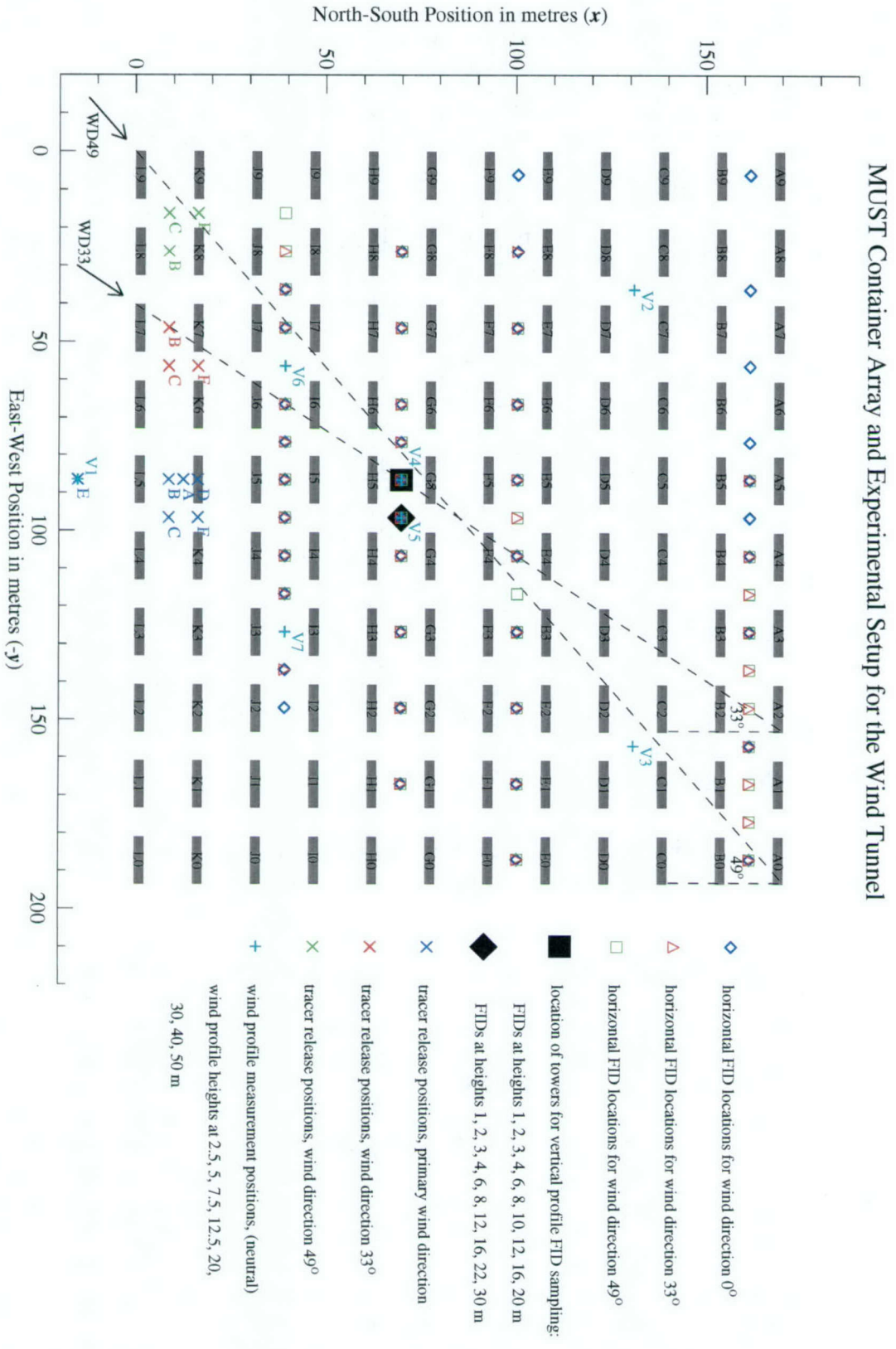

Figure 2.3: Diagram of the MUST container array, as set up for the wind tunnel, including wind directions (dashed lines), source release points (cross with letters), and sampling locations (symbols). Length scales are given in equivalent full-scale coordinates.

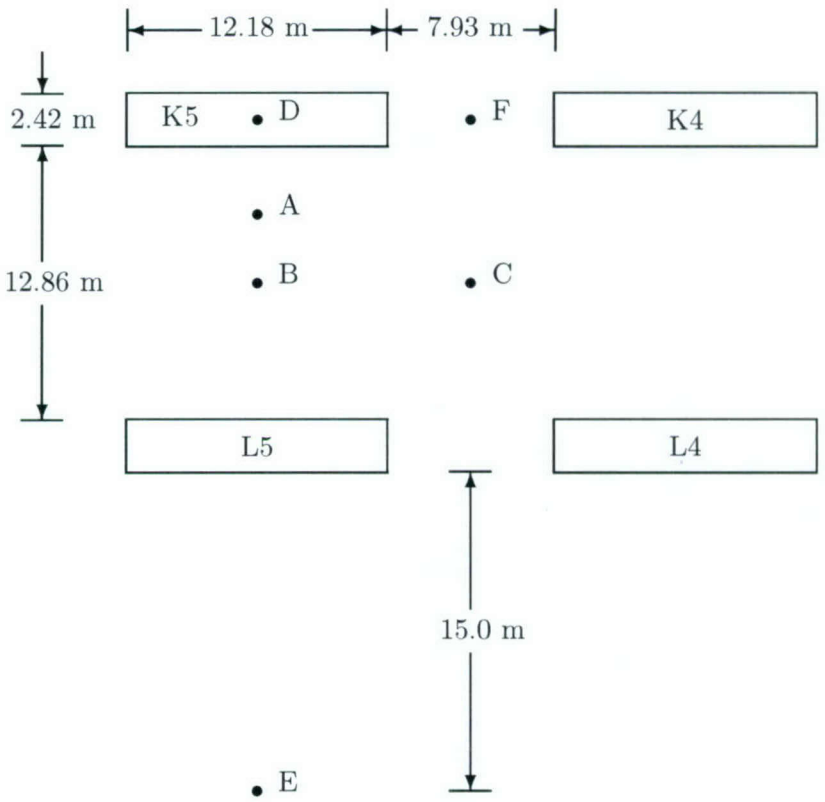

Figure 2.4: Layout of 4 containers in the MUST array, showing the dimensions and relative spacing between obstacles, as well as the source release position types. Dimensions are given as the full-scale equivalent distances.

The obstacles were cut out of foam, and glued onto a number of plyboard base sections, which were then positioned on the wind tunnel turntable in the test section.

2.3 Model Scaling

To successfully model the dispersion around full-scale structures in a wind tunnel, it is important to achieve kinematic and dynamic similarity of important parameters in the model as compared to full-scale. We concentrate at present on scaling in neutral conditions, which is the atmospheric stability category investigated for the majority of trials in the current investigation (see Section 2.4 for further discussion of atmospheric stability). It turns out that the scaling arguments presented here for neutral conditions will also apply well to tests in stably stratified flows, of which a limited number were done in the current set of experiments. This is due to the simple properties of the source and lack of buoyancy in the emerging tracer. These scaling arguments have been developed for the application of dispersion modelling of tall industrial chimney stacks emitting buoyant pollution, hence the nomenclature used below. The theory is further discussed, for example in [17]. There are essentially three parameters which are important to keep constant between model and full-scale, namely the momentum parameter, buoyancy parameter and mass flow rate ratio. We discuss each of these in turn.

The momentum parameter is the ratio of plume to free-stream momentum flux. An initial plume emanating from a release point (such as a chimney stack or in the present case, simply a release hose capped by some sponge) has a finite width d, which by convention we will call the stack diameter. We will denote the mean free-stream horizontal wind velocity by u (measured at 1.0 m in the experiments and parallel to the x-axis for all flow measurements). We also identify a typical length scale of the problem L, which can be taken as the canopy height H for the MUST array. Given an effluent density ρ_g, air density ρ_a and vertical effluent velocity w, the momentum parameter given by the ratio

$$M_r = \frac{\rho_g w^2 d^2}{\rho_a u^2 L^2} \tag{2.1}$$

must be the same in both model and full-scale. In the current trials, the effluent velocity was reduced practically to zero by capping the end of the outlet hose with some porous sponge. Thus we may take $w \approx 0$ for the trials, and thus $M_r \approx 0$.

The buoyancy parameter is the ratio of buoyancy to free-stream momentum flux, and plays an important role for releases of hot effluents and in convective conditions. It is dependent on the density difference of air and the hot gas $\Delta\rho = \rho_a - \rho_g$. Thus, the buoyancy ratio

$$B_r = \frac{\Delta\rho\, dgw}{\rho_a u^3}, \tag{2.2}$$

where g is the acceleration of gravity, must be maintained equal in model and full-scale. In the current trials, the effluent is always of density approximately equal to air and $w \approx 0$, so that $B_r \approx 0$.

The only parameter of significance is consequently the mass flow rate ratio, which is the ratio of mass flow rate of discharge to free-stream flow. Given the source flow rate Q, this is given by

$$F_r = \frac{\rho_g w d^2}{\rho_a u L^2} \text{ or } \frac{\rho_g Q}{\rho_a u L^2}. \tag{2.3}$$

If we consider concentration expressed as a volume fraction, a concentration ratio C_r of model (C_m) to full-scale (C_{fs}) must be equal to unity, i.e. $C_r = C_m/C_{fs} = 1$. Thus a ratio of (volume fraction) concentration C (where C can be either C_m or C_{fs}) with the mass flow rate ratio gives an invariant *dimensionless* concentration parameter

$$K = \frac{CuL^2}{Q}. \tag{2.4}$$

The dimensionless concentration parameter is valid as an invariant quantity if one is trying to achieve only kinematic similarity. This means that mixing is dominated by turbulent diffusion, and there is no dependence on buoyancy or momentum flux (such as in bending over of a plume or convective mixing). The great utility of the dimensionless concentration parameter K is that given one model run, it can be applied to variations in the full-scale wind speed, length scale and source flow rate, and can thus model a wide range of possible full-scale parameter combinations.

For comparison with other trials, concentration data for the MUST wind tunnel experiments is expressed in terms of K calculated from experimental quantities expressed in S.I. units. If we consider tracer concentration measured in some volume, let us denote

the actual tracer volume fraction by V_g, and the air volume fraction by V_a. Then given a concentration C measured in ppm in the experiments, it can be expressed in S.I. units by the relation

$$C = \frac{V_g}{V_a + V_g} \times 10^6 \,[\text{ppm}] = \frac{\rho_g V_g}{V_a + V_g} \,[\text{kg m}^{-3}].$$

This leads to the relationship between K calculated by experimentally determined parameters, and K calculated in S.I. units:

$$\begin{aligned} K[\,\text{dimensionless}\,] &\equiv \frac{C\,[\text{kg m}^{-3}]\,u\,[\text{ms}^{-1}]\,L^2\,[\text{m}^2]}{Q\,[\text{kg s}^{-1}]} \\ &= 60 \times \frac{C\,[\text{ppm}]\,u\,[\text{ms}^{-1}]\,L^2\,[\text{m}^2]}{Q\,[\text{cm}^3\,\text{min}^{-1}]}. \end{aligned} \tag{2.5}$$

2.4 Test Flows

Most wind tunnels operate purely under conditions of neutral stability, where all turbulence is mechanically generated. Buoyancy induced turbulence, intrinsic in most realistic atmospheric flows, requires special design in a wind tunnel. Heating elements are required for the simulation of convective flows, and large tunnels are required to achieve the necessary model to full-scale similarity conditions (see for example [18]). Stably stratified flows, with the temperature inversion profile, require either floor refrigeration, or an alternate method described below.

Since thermal forcing is unnecessary for neutrally stable trials, they are the easiest to set up and perform in the wind tunnel. An appropriate boundary layer is simply developed by the use of various flow conditioning devices upwind of the test section, which generate mechanical turbulence. Consequently, by far the greatest number of tracer releases were done under neutrally stable conditions for the current set of experiments. The full-scale MUST trials however, were generally done under stably stratified night time desert conditions, and atmospheric conditions only occasionally approached true neutral stability. To model stable stratification within the tunnel, physical models need to be attached to the ceiling. The stable stratification is achieved by a set of heating elements located on the ceiling upwind of the model. Air passing over these heating elements is then hotter than the underlying layers, and remains at the ceiling due to buoyancy. This creates an inverted stable layer, trapped at the ceiling under the low wind speed conditions.

Conducting experiments under stable stratification is a fairly time consuming and difficult process, with the further limitation that no turntable is available on the ceiling to test a variety of wind directions. It was also expected that turbulence generated by the obstacle array would dominate the dispersion processes, so that the effects of atmospheric stability would not be as important as for dispersion in open, unobstructed terrain. The experimental design did however wish to establish a link between the bulk of the tests performed in the wind tunnel under neutral stability conditions, and the predominant conditions experienced in the full-scale MUST trials. Thus although expensive to do, a limited set of stably stratified trials were undertaken in the wind tunnel, to test the effects of atmospheric stability on the dispersion within an obstacle array.

2.5 Instrumentation

Pure ethylene was used as the tracer in the experiments. The density of pure ethylene is very similar to that of air, so that the releases had neutral buoyancy, and very little vertical momentum (see the discussion of buoyancy in Section 2.3). 12 flame ionisation detectors (FIDs) were available for sampling. These detectors consist of small filaments through which contaminated air is drawn by vacuum. The gas is then ionised in a combustion chamber, which produces an output voltage ranging from -10.0 V to +10.0 V. This output signal is converted to a digital time series (given in 12 bit a/d levels), through an a/d board. The signals passed to the a/d board were low-pass filtered to 33 Hz, and digital output was sampled at 100 Hz. Due to the sensitive nature of the FIDs, it was not always possible to have all 12 functioning at once. They routinely required unblocking and maintenance, so that it was decided to have 10 FIDs sampling at any one time. This provided a fairly consistent dataset, with always the same number of channels in operation. Unfortunately at times some of the operating FIDs did drop out, so that some of the sets of concentration time series had spurious channel signals. The ends of the FIDs were mounted on small stands, which corresponded to a height of about 1.8 m in full-scale. This height is very close to the actual height that samplers were mounted in the full-scale MUST trial. The FIDs were housed in chambers mounted on a traverse system. This system was able to be electronically controlled from the operating room, and referenced to a fixed wind tunnel coordinate system. The traverse could be moved in either the x, y or z direction through the manipulation of switches, and the sampling filaments of the FIDs could be located anywhere within the test section of the wind tunnel. See Figure 2.5, for a photo of the wind tunnel MUST array, including the FIDs and their associated chambers, and the filaments attached to sampling stands within the array.

Calibrations of the FIDs were generally only done once per day, usually at the end of each day of the experiments, or where a convenient break in the setup of the experimental programme occurred within a day. The calibrations essentially involved measuring a set of known quantities of ethylene, and thus deriving a linear relationship between the sampling instrumentation output in millivolts (mV) to a concentration in parts per million (ppm). A daily calibration of the FIDs was necessary, as significant changes (over 10%) in the calibration of any given channel could be noticed from one day to the next. It was also possible for a calibration to change slightly throughout a day, but this change was generally expected to be less than 10%. Ideally at least two calibrations should have been made per day, but this proved difficult given the time constraints of the experimental programme. Calibrations done later in the day were usually taken to be more reliable, as the FIDs required some time to warm up properly. An appraisal of the uncertainty in the calibrations, based in part on previous calibration data of the FIDs, is given in Section 4.3. The actual calibration spreadsheets for the experiments are contained on the data CD under the directory `/results/calibrations`.

Detailed flow measurements were made using crossed hotwire anemometers, in conjunction with a digital vane anemometer used to provide a reference mean wind speed. Hotwire anemometers are not suitable for use in strongly recirculating flow regions. The reason for this is that they are very sensitive to fluctuations of temperature, which then correspond to the measured wind speed fluctuations. They consequently measure only scalar fluctuations, and cannot account for variations in wind direction. Thus aspects

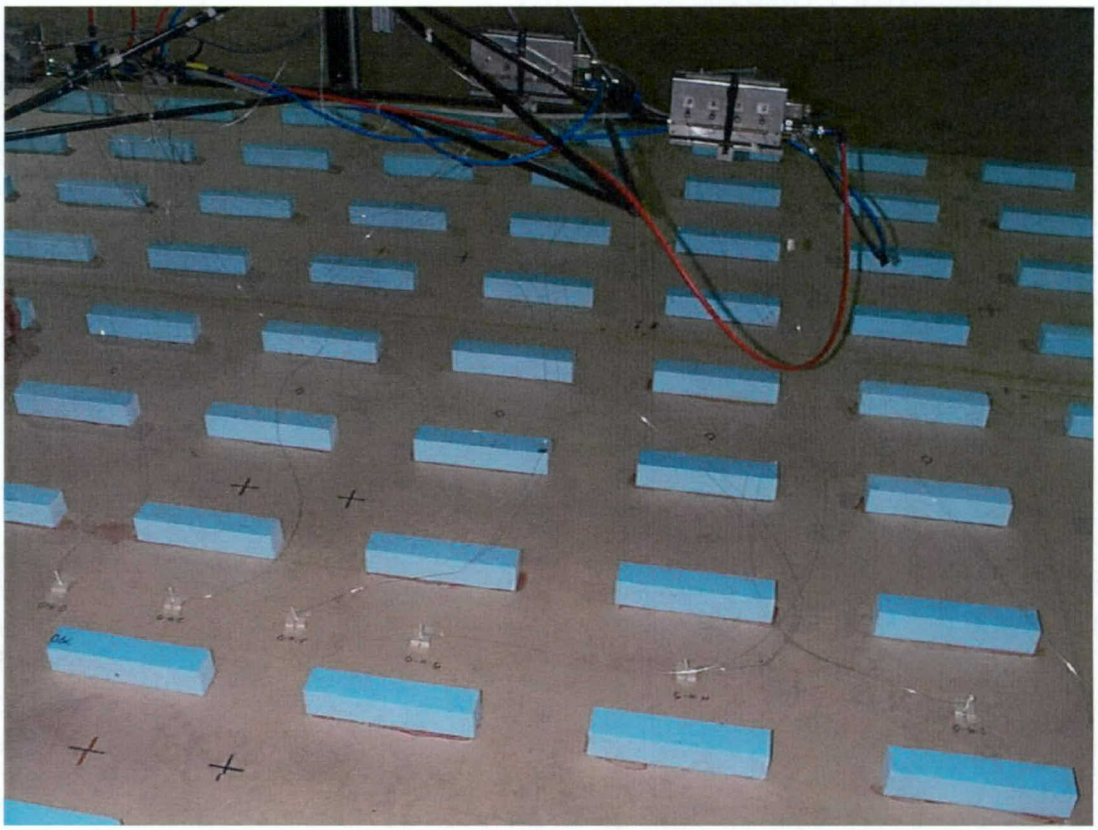

Figure 2.5: A photo of the wind tunnel model of the MUST array, showing the FIDs mounted on a traverse, and the sampling filaments attached to stands in the model.

of highly turbulent flow such as flow reversal would not be correctly measured by the hotwires. This meant that profiles could unfortunately only be taken above the obstacle array, and no velocity measurements are available within the actual MUST array canopy. The crossed wires measured two wind components simultaneously, and the directions that were initially chosen were the u-w (streamwise and vertical) components. Some time permitted to make limited measurements of the u-v (streamwise and transverse) components by changing the orientation of the crossed wires. The output of the hotwires were raw voltage signals, which were calibrated with the mean wind speed measured by the co-located vane anemometer. The hotwires were useful for deriving higher order turbulence statistics such as turbulence intensity, and for obtaining velocity spectra. They ultimately allowed a detailed characterisation of the boundary layer profile established in the wind tunnel, and to see the effects and perturbation on the upwind boundary layer caused by the MUST obstacle array.

2.6 The Wind Model

The first task to achieve in the accurate model simulation of the atmosphere was the creation of the correct boundary layer wind flow model under neutrally stable conditions. The full-scale test site comprised flat desert terrain, with some significant desert bushes scattered throughout the domain contributing to a roughness length z_0 of about 5 cm.

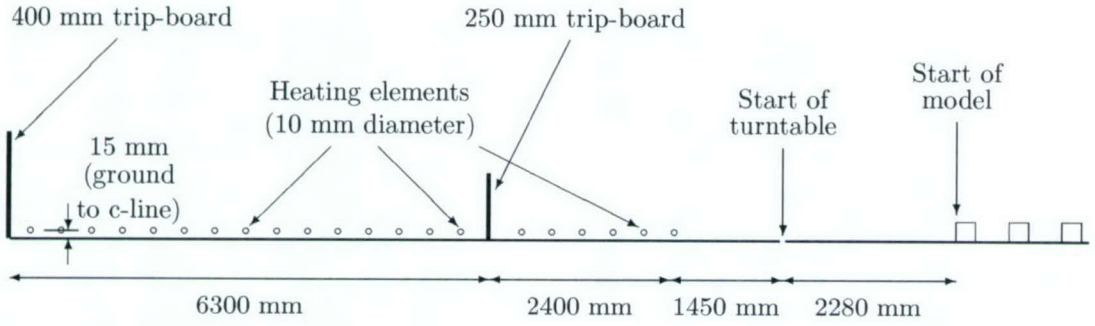

Figure 2.6: Longitudinal (x-z section of the layout of the upwind flow conditioning elements for the boundary layer wind model. The vertical scale is exaggerated.

This type of terrain was modelled in the wind tunnel using the Australian Wind Loading Code (AS 1170.2-1989) [19]. The corresponding category in this case corresponded to wind code category 2—desert landscape. Trip boards of width 400 mm and 250 mm were placed in succession upwind of the test section to act as vorticity generators, which in conjunction with the heating elements on the floor acting as roughness, accelerated the stream-wise development of the larger scale eddies in the boundary layer flow (see Figure 2.6 and also the photograph in Figure 2.2 for a visualisation). This produced mean and turbulence velocity profiles that matched fairly well with a desert landscape, as described in AS 1170.2-1989. These profiles are based on work by Deaves and Harris [20], which consists of some classic measurements of wind and turbulence profiles. Figure 2.7 gives an illustration of the tunnel measured vertical wind profiles, including (a) mean wind speed $u(z)$ and (b) longitudinal turbulence intensity $i_u(z) = \sigma_u/u$ (where σ_u is the standard deviation of velocity in the direction of the mean wind). The profiles were measured at position V1 (see Figure 2.3), upwind of the array. The measured values have been scaled in relation to the standard AS1170 category profiles, which are expressed as a multiplying factor of wind speed scaled to 500 m height. A reference velocity at 1.0 m measured in the tunnel was taken, and scaled to match the AS 1170.2-1989 terrain category 2 value at the corresponding 50 m full-scale height.

The mean wind velocity profile $u(z)$ could be fit fairly closely by the power law profile

$$\frac{u(z)}{u_{50}} = \left(\frac{z}{50}\right)^{0.14}, \tag{2.6}$$

where $u(z)$ is measured in ms^{-1}, and u_{50} is a reference mean wind speed at 50 m full-scale. Reference wind speeds quoted in this report for the dispersion measurements are taken at a model reference height of 1.0 m, and the above relationship can be used to extrapolate wind speeds at different heights. The exponent value of 0.14 corresponds closely to the value of 0.15 specified for terrain category 2 in AS 1170.2-1989. Using graphs found in AS 1170.2-1989 for interpolating between the empirically measured power law profiles of the wind code, and the more fundamental log-law profile usually assumed for the surface layer, the exponent value of 0.14 corresponds closely with a roughness value z_0 of about 2 cm in full-scale. This is lower than the actual value of 5 cm estimated for the full-scale trials, but at least in the same general regime of terrain types, so that modelling of the boundary layer is considered to be quite realistic. A kink in the turbulence intensity profile at approximately the height of the second trip board (12.5 m full-scale or 25 cm model

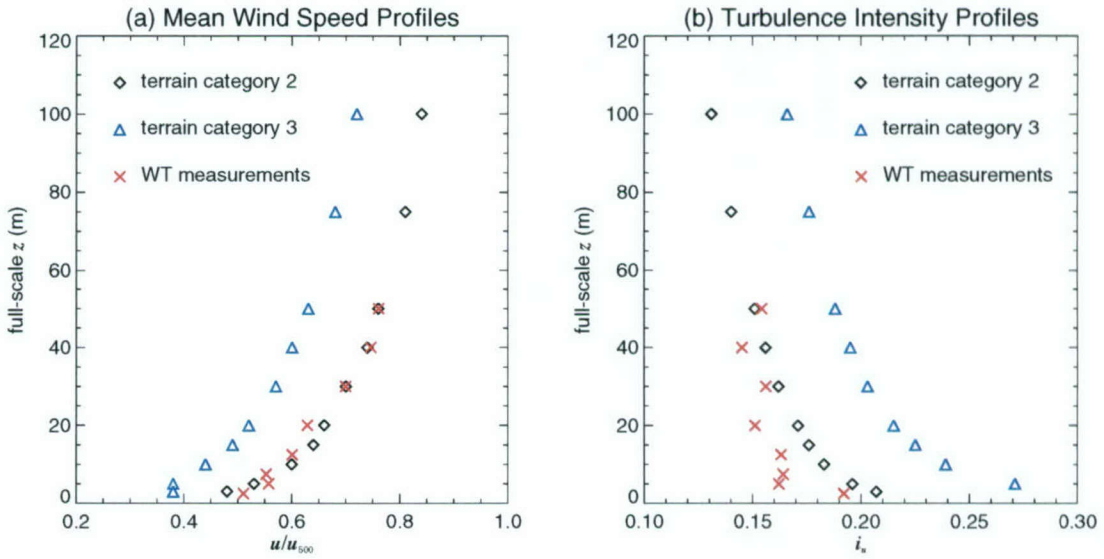

Figure 2.7: Mean wind speed (a) and turbulence intensity (b) profiles for the MUST boundary layer wind model, as measured in the wind tunnel. Heights have been converted to full-scale dimensions to enable the comparison of the measurements with some standard AS 1170.2-1989 terrain categories.

scale) may be noted. This is most likely due to insufficient room being available between placement of the trip boards and the actual scaled model location. These type of artifacts in artificially produced flow models are very difficult to completely avoid.

In general for atmospheric surface layer wind profiles, the wind speed may be plotted against $\log z$, to test for the existence of the standard inertial sublayer "log law" profile

$$u(z) = \frac{u_*}{\kappa} \log\left(\frac{z - d_s}{z_0}\right).$$

The displacement height d_s is always a very poorly determined quantity in such a procedure, as a careful Bayesian uncertainty analysis can show (a very wide posterior density for d_s results[1]). Thus we will assume d_s to have negligible effect in the specification of the upwind profile (also considering that trip boards were used to accelerate boundary layer development, with minimal explicit surface roughness elements being used). The quantity u_* is the surface friction velocity, and the universal Von Karman's constant is usually taken to be around $\kappa = 0.4$. For wind tunnel experiments, a determination of the roughness and friction velocity parameters is usually very difficult by this method, and leads to unreliable results. This is due to the inability to get sufficiently detailed measurements very close to the surface, and the subjectivity involved in selecting which measurement points to include in the logarithmic fit of the constant stress layer. Graphs to extrapolate measured power law profiles to the surface, and inference of the surface parameters by a wind code (such as AS 1170.2-1989) is the preferred method for wind tunnel experiments.

To serve more as a qualitative indication of the surface characteristics rather than a detailed quantitative analysis, two measured profiles are further investigated here. The

[1]Personal communication from Dr. E. Yee, DRDC (Suffield), Canada

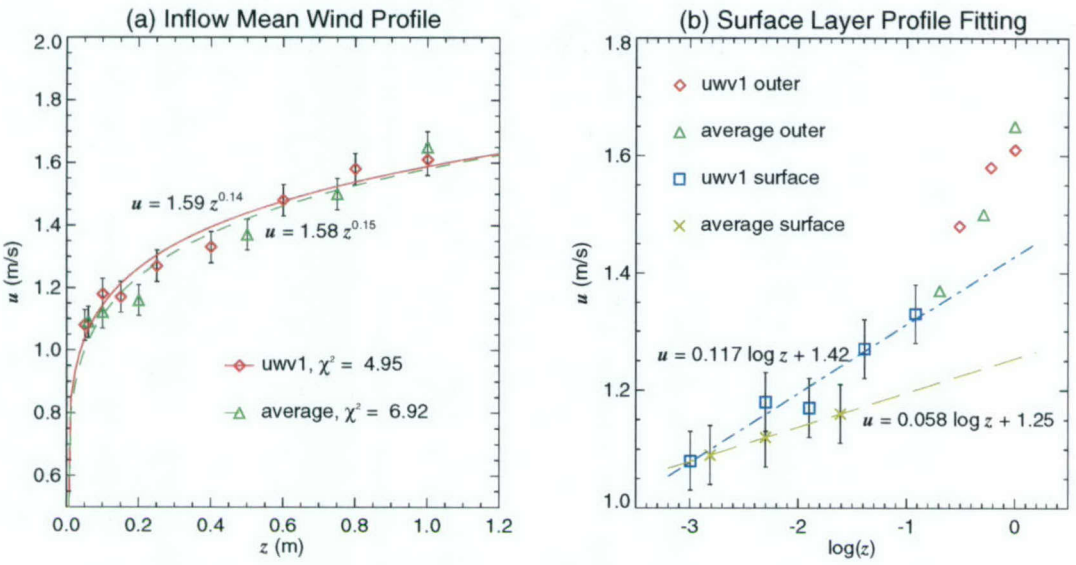

Figure 2.8: Power law fitting to the mean wind profile (a), and investigation of the surface layer with a log law profile (b) for the MUST boundary layer wind model.

first was that originally measured and used as the definition of the tunnel inflow conditions when the boundary layer was being characterised, which will be called the "average profile" (alluding to the average taken over a number of repeated measurements). The second, which will be called "uwv1", refers to one of the set of detailed velocity time series measurements made later in the trials using hotwire anemometry and the vane anemometer simultaneously, from which a mean velocity profile was extracted. Figure 2.8 shows both the mean wind speeds fitted with power laws over the full range of measurements (a), and logarithmic profiles fitted in a region that appeared to be a constant stress layer (b). Although there is some scatter in the data, the measured mean wind power law profiles show good consistency for the two cases considered, with the value of the exponent in the range $0.14 - 0.15$ (Figure 2.8(a)). Calculated χ^2 values are based on assumed standard uncertainties of $\pm 0.05\,\mathrm{ms}^{-1}$ for all the plotted data points. This is simply a reasonable estimate of uncertainty based on the variation found in the limited number of repeated measurements made. The χ^2 values show acceptable levels of confidence for the assumption of a power law form to the profiles.

Due to the limited number of measurements, there is some subjectivity and considerable uncertainty in identifying the constant stress layer region. It can only be roughly located from what appears to be the most linear section of the data plotted on semi-log axes (see Figure 2.8(b)). It is clear that the slope of the line is difficult to define, and depends on the subjective choice of points to include in the constant stress region. This is demonstrated by the marked difference in the slope for the two profiles fitted in Figure 2.8(b). Values of the friction velocity calculated from these two fitted lines come out in the range $u_* = 0.047\ \mathrm{ms}^{-1}$ for "uvw1", and $u_* = 0.023\ \mathrm{ms}^{-1}$ for "average profile". The roughness length z_0 is very poorly determined, since it is exponentially dependent on both the slope and intercept of the fitted line. The two datasets fitted above gives several orders of magnitude difference in their prediction of z_0. We thus ignore the deduced value of z_0 obtained from this method, and appeal to the value of 2 cm as derived from the wind

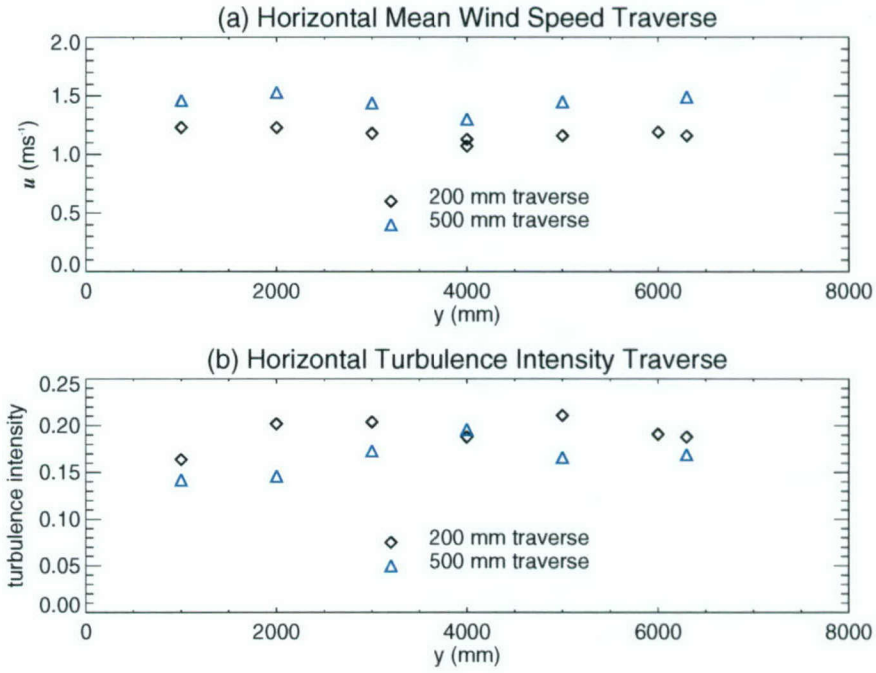

Figure 2.9: Horizontal mean wind speed (a) and turbulence intensity (b) profiles for the MUST boundary layer wind model. Traverses were made at heights of 200 mm and 500 mm.

code.

Traverses of the tunnel in the cross-wind (y) direction were also made at two heights of 200 mm and 500 mm, to test for the horizontal homogeneity of the flow. The results of the measurements are shown in Figure 2.9, in which the actual model scale measured mean wind speeds (a) and turbulence intensities (b) are plotted. The traverses were made at the upwind edge of the turntable, and show a span of 8.0 m across the centre of the tunnel, with the left-hand edge ($y = 0$) aligned with the left-hand edge of the 8.0 m diameter turntable, (looking in the downwind direction). Looking at the statistics of the set of horizontal wind measurements shows that the scatter (standard deviation) of the ensemble of mean wind speeds measured across the tunnel is at about 5% of the mean value of the ensemble. The turbulence intensity scatter is about 10% of the mean value across the tunnel. Given that the expected experimental scatter in these measurements is of a similar order, the profile can be considered to be reasonably horizontally homogeneous. The turbulence intensity is reduced to some degree near the side walls as must be expected by the restriction of scales of turbulence near the boundary. The same effect is inevitable in any wind tunnel.

The stably stratified boundary layer was also characterised in a basic way, essentially to give an indication of the level of stability. Using a small number of measurement points of temperature and mean wind speed close to the surface, an approximate linear temperature gradient of -5.9 deg/m was established (negative because of the upside down model, which produces negative buoyancy in the inverted frame of reference, and hence stable stratification). Using these measurements, it was possible to compute a bulk Richardson number to indicate a level of stability. This dimensionless number gives a measure of the

relative strength of buoyancy forces to mechanical turbulence forces (see e.g. [21]). Its definition is

$$R_b = \frac{(g/T_z)(T_z - T_0)/z}{(u(z)/z)^2}, \tag{2.7}$$

where T_z is the mean temperature at height z (the difference between potential and absolute temperature is negligible on these scales), g is the acceleration due to gravity, and T_0 is the temperature at the surface. The value of R_b calculated at 55 mm, the lowest measured height of temperature and wind speed, was found to be 0.033. This value, measured just above canopy height, indicates a stable layer (for which $R_b > 0$ is required), and shows that the layer is considerably turbulent. A turbulent stable boundary layer is assured for R_b below the critical Richardson number $R_c \approx 0.25$. Values of R_b between 0.25 and 1.0 can lead to a mixture of laminar and turbulent layers, and values above 1.0 indicate a flow that is definitely laminar.

2.7 Test Programme and Measurements

An outline of the type of measurements made, together with source and sampling locations, wind directions and other physical parameters is given in this section. All except one of the dispersion trials used constant, continuous releases of material. A far greater quantity and variety of information could be extracted from the continuous release data, due to the ease and speed of setting up and running different configurations. The one puff trial discussed below was relatively expensive in terms of time and effort in obtaining data for just a single release configuration and sampling line of detectors. Some initial tests were conducted in an attempt to determine an optimum sampling time for the continuous releases, and to check various dimensionless scaling hypotheses. These tests will be discussed in detail in Section 4.5, but here it is noted that all continuous releases were sampled for 600 seconds except one or two, where some FIDs dropped out before the complete time period passed. The release rate of material varied from trial to trial, depending on the distance of the sampling line downwind. Practical limitations on the sensitivity of the FIDs required much greater source release rates for sampling lines further downstream of the source.

Three wind directions were considered for measurements of dispersion in the wind tunnel experiments: 0, 33 and 49 degrees relative to the columns of the array (x-axis). These wind directions will henceforth be referred to as wd00, wd33 and wd49. (The full-scale trials of course had a great variety of wind directions covered in the complete dataset.) The oblique wind directions wd33 and wd49 are indicated by dashed lines in Figure 2.3. Corresponding to each wind direction were a number of different release positions of tracer gas, labelled A–F. Each set of release locations is colour coded according to wind direction: blue for wd00, red for wd33, and green for wd49. Corresponding to these wind directions are lines of samplers at several downwind distances, with the sampler locations for the wind directions distinguished by colour and a specific symbol. Specifically, the sampling lines will be referred to as rows IJ, GH, EF and AB, indicating their position relative to the rows of containers. These sampling lines correspond closely to the sampling lines set up in the full-scale trials, with the exception of the last row AB. For the wind tunnel experiments, it was felt that maximum use should be made of the array, hence the use of this sampling line. For full-scale trials this was obviously not possible, due to the unpredictability of the

wind direction. A large black square box also indicates the position of a vertical sampling tower, corresponding to the same position of the vertical tower used in the full-scale trials. Samplers were located at heights of 1, 2, 3, 4, 6, 8, 10, 12, 16 and 20 metres (full-scale) on this tower. Most vertical profiles were made on this tower, but a second neighbouring tower (black diamond) was also used in several trials for comparison purposes. This tower had samplers located at heights 1, 2, 3, 4, 6, 8, 12, 16, 22 and 30 metres (equivalent full-scale height), in an attempt to capture some of the intermittent bursts of concentration that were still surprisingly being detected at the higher levels. The 30 metre tower had no full-scale equivalent.

Figure 2.3 also indicates the position of flow measurement profiles, indicated by pale blue plus symbols. At each profile position in the array, time series of velocity fluctuations were collected at equivalent full-scale heights of 2.5, 5, 7.5, 12.5, 20, 30, 40 and 50 metres using the crossed-wire anemometers in conjunction with the vane anemometer. The vertical sampling profiles were labelled V1, V2,..., V7, as indicated on the diagram.

One set of puff releases was also done for the primary wind direction of interest (wd00). The puffing mechanism consisted of a cylindrical container, open at the bottom, which sat on a mounting plate attached to the ground. A hole was drilled through the mounting plate and the floor of the wind tunnel, and the inlet hose was connected to the puffing mechanism through this hole and a valve, so that material could be injected into the container. There was a tight seal between the cylinder and the mounting plate to contain a fixed volume of material. The cylinder could be rapidly lifted away from its mounting plate to leave a suspended puff of material in the path of the flow, ready to be dispersed downwind. As the puff was released, the valve was also simultaneously closed to stop further material from entering the puff. In this way, a neutrally buoyant puff with no initial momentum could be produced. It is expected that minimal skin friction existed between the parcel of material contained within the container and the very smooth walls of the container, so that lifting of the cylinder would cause negligible vertical momentum of the puff. Release of the puff also triggered a data collection computer to begin sampling the FID output, so that all time series collected began exactly at the time of release of the puff.

Some practical difficulties did exist with the puffing mechanism. One problem was the fact that it was extremely difficult to produce a perfect seal on the puff container, so that there was always a little leakage of material before the puff was actually released, contributing a small but noticeable signal to each puff time series. The size of the puff cylindrical container was also an issue in the experimental design. Even the smallest puffer designed had a volume approximately similar to the size of an actual shipping container in the model, and thus was a significant obstacle in the flow. The quantity of material released from such a puff was only reliably detectable in the first sampling line of FIDs, due to sensitivity limitations on the samplers. Thus it was only possible for the first line of samplers (row IJ) to collect data on the puff releases under the experimental release conditions and time available. For good statistical convergence for the results of the puff experiment, it was deemed by past experience and real time ensemble averaging as the set of time series was collected, that at least 50 puffs were required in an ensemble. The actual number collected for the one puff trial was actually 62, and this in itself was a considerably time consuming and expensive part of the entire experimental programme.

3 Data Analysis

3.1 Overview of the MUST Wind Tunnel Dataset

In this subsection, a general description of the MUST dataset will be given, including the organisation of the dataset on CD. The dataset is organised into various directories, the bulk of which comprises the continuous source concentration dispersion data time series and associated files. In addition to this, other directories contain more highly processed data (such as spreadsheets and plots), as well as data processing scripts and other documentation. The time series are all located under the parent directory `data_files`. Under this parent directory, there are data directories labelled `day1, day2, ..., day6`, for the trials done under neutrally stable conditions, and `stable` for the one set of trials done under stably stratified conditions. In addition to this is a directory `npb00ij` containing all the data from the one puff trial conducted, and a directory `vel` containing the velocity time series data. Under the data directories are a number of files corresponding to each individual release and sampling of material. To explain the file naming system, it is useful to first explain in a little more detail how the data was collected.

The data acquisition system consisted of a 12 bit a/d board, writing a/d levels to file in 16 bit integers ranging from 0 to 4095. In terms of measured voltages, $0 = -10.0$ volts, $2048 = 0.0$ volts, and $4096 = 10.0$ volts. Each time scan of the a/d board gave off 12 integers (24 bytes) for each of the 12 FID channels, and packed a 32 byte record written to file with 4 extra channels of zero data (8 extra bytes). With 100 Hz sampling for periods of 600 sec, raw data files collected were generally approximately 1.9 MB in size. Since only 10 FIDs were actually ever sampling concentrations within the model at any one time, data processing scripts were written to strip out the 4 extra packing channels, as well the 2 spurious FID channels recorded for every run. Thus all time series files contained on the data CD consist of 10 columns of 16 bit integer binary data, with values ranging from 0 to 4095.

Each binary data file has a base file name (notation explained below), with a `.bin` extension. Accompanying each of these files are several "configuration" files of ASCII data, with the same base file name but different extension. A simple list of used channel numbers (10 integers between 1 and 12), in the order recorded in the `.bin` file is given in the `.chn` file. The `.bas` file gives baseline a/d level correction for each channel listed in the `.chn` file as a real number. Baseline correction of the time series is discussed in detail in Section 3.3. Finally, there is a `.txt` file corresponding to each binary data file, giving some common statistics calculated for each channel time series.

The naming system for dispersion measurement files involves file names of 8 characters in length, with each character describing a particular aspect of the experimental configuration, as described below:

char1 (values `n` or `s`): described the trial as being either neutral or stably stratified.

char2 (values `c` or `p`): described the release as either continuous or puff

char3 (values `a`, `b`, `c`, `d`, `e` or `f`): gives the release position type

char4 and char5 (values 00, 33 or 49): gives the wind direction

char6 and char7 (values ij, gh, ef, ab, ve or vx): describes the sampling line as either the 4 horizontal rows, the 20 m vertical tower (ve), or the 30 m vertical tower (vx).

char8 (single digit integer): distinguishes different runs of the same experimental configurations, such as repeated runs testing for statistical convergence; the same configurations with different wind speeds or source release rate were also possible. The most common number of 2 indicated a wind tunnel fan speed of 100 rpm. (Other values included 1 for 50 rpm, 3 for 200 rpm, and still other values if more repeats were done).

As an example, consider the trial called ncb00ij3. This trial was performed under neutral flow stability, the source release was continuous, and the release type was B. The wind direction was wd00, the sampling line was in row IJ, and it was the third run in a set done under the same setup just specified (with 200 rpm wind tunnel fan speed). Associated with this run are the following files:

1. binary time series data file ncb00ij3.bin,
2. ASCII file listing the channels used, ncb00ij3.chn,
3. ASCII data file containing the baseline a/d level corrections to the raw binary data files, ncb00ij3.bas (expressed as real numbers),
4. and an ASCII summary statistics data file, ncb00ij3.txt.

A similar collection of files followed for all the velocity profile time series collected. The actual base filename convention was however slightly different. The first two characters in the name were either uv or uw, depending on whether the crossed wires were aligned to simultaneously collect the u-v or u-w components of velocity respectively. The third and fourth characters took the values V1, V2, V3, V4, V5, V6 or V7, to indicate which of the seven possible profile sampling positions were used (see Figure 2.3). The last four characters give the vertical height of the measurement location, given in millimetres above the wind tunnel floor. Thus for example, file uwv30250.bin contains time series in binary form of the u-w components of velocity at vertical sampling position V3, with the measurement height of 250 mm. The first two time series in a binary data file contain directly measured time series of the crossed wires, which are aligned at 45° in either the u-v or u-w planes. This is necessary to obtain substantial signals for each components. The third and fourth time series in the data file contain the correctly rotated u-v or u-w time series of velocity, obtained by forming the sums and differences of the first two channels. The same supporting .chn and .bas file are also present for each binary data file.

Appendix B gives a complete list of all the binary data files collected, including the basic experimental configuration associated with each file.

3.2 Real Time Analysis

To enable data quality monitoring and the ability to determine the optimum experimental parameters, it was highly desirable to have a real time data analysis capability

throughout the trials. The wind tunnel facility offered its own in-house software for viewing incoming data, which was sufficient for the wind tunnel operator, but not for monitoring the quality of the experiments and for making decisions about how to steer the direction of the trials in real time. In particular, there was no facility for plotting and analysing the full time series data, and manipulating ensembles of time series (as for puff releases).

Some real time data analysis scripts were developed using the propriety scripting language FAN [22] (Kosteniuk Consulting—Saskatoon, Canada), designed explicitly for the analysis of time series and signal processing, particularly for atmospheric dispersion experiments. The scripts developed had the ability to convert between the raw output of the sampling computer to a more compact and useful binary representation of the data, and simultaneously plot the output of all incoming data channels as a set of time series. Also included in the scripts were some basic statistical analysis routines and baseline correction tools to obtain preliminary plots of mean concentration profiles and related data. This facilitated in monitoring the validity and usefulness of the current stage of investigations in the trials. Ensemble averaging tools were also developed, in order to determine the optimum number of releases for an ensemble of puffs. These real time analysis scripts are available in the `/scripts` directory, and are comprised of the files `rview1`, `view1.cfg`, `view1.pan` and `view1.mac`.

3.3 Baseline Correction

The raw output signal from the FIDs had no significance attached to the actual zero voltage readings. The true baseline (actual a/d level corresponding to zero concentration) had to be determined from the information at hand during the experiments. "Zero runs" were periodically performed during the trials, typically after every 3 to 6 individual time series samples (each individual time series corresponding to a 600 second sampling time). This monitored the actual a/d baseline value of each FID channel, which could change as a result of background accumulation of concentration in the tunnel, or some other unknown reasons in the response of the FIDs. Zero runs involved sampling the background air in the tunnel for 60 seconds, and averaging the time series for these samples to determine the mean of the baseline noise. The baselines typically were quite stable, with low noise. They tended to reveal fluctuations about the mean of only one or two a/d levels.

At times it was possible for the baseline to drift over a 600 second sampling period by one or two a/d levels. This generally seemed to happen more earlier in a day of trials, maybe because the FIDs took time to warm up, or because a background equilibrium of contaminant in the tunnel took several hours to become established. On the scale of readings taken, the baseline drift of one or two a/d levels per sampling period was very low, and consequently it seemed sufficient to determine a single value of the baseline for each time series collected, rather than to fit a spline or use some other more complicated method to produce a very detailed picture of the baseline.

Nevertheless, within a period of 3 to 6 sampling sets, the baseline value for each channel could vary significantly from one trial to the next. Thus the baseline value of intervening time series between two zero runs had to be deduced from examining points in the time series where the signal "bottomed-out" (appeared to reach a regular minimum value), or by interpolation between the values obtained from zero runs. It was generally possible to

pick where the zero concentration level lay by examining the zero spikes in the time series, as the signals were generally intermittent enough on a regular basis to see a succession of such spikes consistently dropping to a certain level. It was also generally possible to see some small drift in these regular zero concentration points, if it was present. For sampling channels near the edge of plumes, it was very simple to obtain an accurate baseline value, since the signals were very intermittent, with long periods of fluctuation around a baseline value. In the centre of a plume, signals were far less intermittent, and there was greater uncertainty attached to the baseline value. When the baseline value tended to fluctuate somewhat from trial to trial, it was tempting to make more frequent zero runs. This had the downside that the valve controlling the source flow rate had to be turned off, and when it was turned on again, the flow rate always took some time to stabilise. This would add extra uncertainty to the source flow rate, and would only marginally be offset by improved determination of the baseline values. Thus the balance of a zero run every 3 to 6 time series had to be struck.

Determination of the full set of baseline values for all time series collected was a tedious and time consuming task, so that some methods to automate the procedure were investigated. Two simple algorithms were devised and tested. The first, which had largely been used in a previous trial in the same tunnel, was to simply add a fixed amount to the lowest a/d level detected. Thus if it was believed that the noise around the baseline value generally fluctuated by one a/d level, the baseline value applied to any particular time series would be just the lowest detected level plus one. This method proved quite unreliable when compared against the values obtained for the zero runs, and by more carefully examining the succession of minimum spikes in the time series. Most time series invariably had several isolated instances of noise of amplitude greater than the expected fluctuation around the baseline. In addition to this, noise restricted to a small band around the baseline level generally was not evenly distributed in each a/d level bin, so that determination of a baseline from this method neglected to take into account the correctly weighted mean of a baseline segment—important for times series with longer periods of intermittency. This method's failings may not have been that significant for samples collected within the central area of a dispersing plume, where baseline determination was inherently more uncertain, but in compensation the signal to noise ratio was high. At the edges of the plume however, where the signal to noise ratio was much lower, the baselines needed to be determined with much greater accuracy, to avoid significant biases in mean statistics calculated from the time series.

The second algorithm used a set threshold (usually one a/d level), to define an amplitude or width of the baseline noise. By viewing histograms of the time series, the hypothesis was made that the maximum bin count generally occurred around the baseline level. Then, using the set threshold around this level, a number of a/d bins (a threshold of amplitude one would correspond to three bins) were conditionally sampled. The mean of this conditionally sampled time series would correspond to the baseline level. For time series with some intermittency and a narrow noise amplitude (the majority of time series sampled), the baseline values appeared to be determined quite accurately. If there was greater baseline drift in a particular series, more uncertainty had to be attached to the method, and for some signals with very little intermittency, the method obviously failed. This method can clearly only work for signals with unimodal single point probability density functions (PDFs), peaked around the baseline (generally exponential or clipped

Gaussian PDFs). The cases that did not work as well tended to include very well–mixed portions of a plume, further downwind of the source, and particularly the stably stratified trials. For stably stratified trials, the dispersing plume was presumably quite vertically restricted, and thus yielded higher concentration values, more mixing and less intermittency within the obstacle array.

In summary, no algorithm tested yielded a full-proof method for accurately determining the baseline levels of all time series from these types of dispersion trials. By carefully examining plots of the baseline portions of the time series, it was usually possible to judge how well a method was performing, and at times the calculated values simply needed some manual adjustment to "look" correct. By keeping the "absolutely true" zero runs in mind as data points that the determined succession of baseline values had to be consistent with, a uniform picture of the drifting of the baseline for each trial day was developed. The baseline level determination procedure was labour intensive and time consuming, but necessary to ensure quality of the overall dataset. When considering an uncertainty analysis of the data later in Section 4, it will be shown that in some instances the baseline uncertainty contributed a significant amount to the overall uncertainty in the value of various time series statistics. Fortunately, this was generally only the case for baseline levels of signals detected at the edges of a dispersing plume, with relatively small signal to noise ratios. For the plume channels closer to the centreline, with a high signal to noise ratio, the relative uncertainty in the baseline levels was generally reduced to a negligible amount, even if the absolute uncertainty in the baseline value was much larger.

The baseline analysis scripts are available in the `/scripts` directory, and are comprised of the files `rbase`, `base.cfg`, `base.pan` and `base.mac`. The `.bas` file associated with each `.bin` data file has been described in Section 3.1. In each data subdirectory, there is also an ASCII file of baseline values, which is essentially a concatenation of all the individual `.bas` files listed under the particular subdirectory. This file then, called `basef.txt`, contains identical values to those contained in all the individual baseline data files, and is believed to represent the best estimates of the baseline a/d offsets. Each column in this file corresponds to a particular channel. The files `base1.txt` and `base2.txt` give corresponding values calculated by the algorithms described above.

3.4 Concentration Time Series Statistics

One of the major tasks in the data analysis was the processing of all trials to extract concentration time series statistics. Given a time series of instantaneous concentration data points $\{x_i\}_{i=1}^{N}$, with the usual value for the current experiments being $N = 60,000$, the statistics considered in the data processing included:

1. mean concentration $\overline{C} = \frac{1}{N}\sum_{i=1}^{N} x_i,$
2. mean square $\overline{C^2} = \frac{1}{N}\sum_{i=1}^{N} x_i^2,$

3. variance $\sigma_c^2 = \overline{C^2} - \overline{C}^2$,

4. standard deviation $\sigma_c = \sqrt{\sigma_c^2}$,

5. fluctuation intensity $i_c = \dfrac{\sigma_c}{\overline{C}}$,

6. skewness $s_c = \dfrac{1}{\sigma_c^3} \sum_{i=1}^{N} (x_i - \overline{C})^3$,

7. kurtosis $k_c = \dfrac{1}{\sigma_c^4} \sum_{i=1}^{N} (x_i - \overline{C})^4$.

All the statistics 2–5 above are related to one another through simple algebraic relations involving the mean, so that only one is required to specify information on the second moment of the time series. Thus only the fluctuation intensity results have been listed in the final spreadsheet collection of data, whereas variance and standard deviation have also been listed in the `*.txt` files (discussed more below). Fluctuation intensity is the most appropriate quantity to tabulate in the final dataset, since it gives a normalised, scale independent measure of the magnitude of the variability in the instantaneous concentration field. Note that the fluctuation intensity i_c has been referred to throughout the data files and processing scripts as the *fluctuation amplitude*. This is in keeping with the convention used in the FAN scripting language manual [22], and also to distinguish the sometimes confusing terminology used in the literature. In most physical contexts, an intensity usually refers to a squared amplitude or quantity (such as $\sigma_c^2/\overline{C}^2$). In this report however, the choice has been made to revert to the usual convention of the dispersion literature, and refer to the quantity $i_c = \sigma_c/\overline{C}$ as the fluctuation intensity.

Actual reduction of the time series data to tables of statistics was a relatively straightforward operation, easy to implement with FAN, which had many in-built commands suited to this purpose. Of a more difficult nature was the analysis of uncertainty in all the extracted statistics. A careful analysis of uncertainty in the results is an aspect of data analysis that usually receives little attention in wind tunnel and atmospheric dispersion experiments, but it was felt sufficiently important to devote considerable effort to it in the current investigation. A detailed appraisal of the uncertainty analysis methodology used will be given in Section 4. A discussion of the motivation behind the detailed analysis will be deferred until then, but it is noted in passing that a careful consideration of the uncertainty in the results provides a rigorous underpinning to the entire dataset.

An analysis of uncertainty had particular value for the derived mean concentration results. Postulated profiles (usually Gaussian) were fitted to many sampling lines for the mean concentration statistics using least squares methods. Having predetermined uncertainty bounds on the data points enabled actual uncertainty weighted χ^2 values to be calculated for each fit, and thus gave a measure of "goodness-of-fit" for all the profiles. Under certain circumstances (particularly the vertical sampling lines), alternative hypotheses were also able to be examined, such as reflected Gaussian profiles

$$\overline{C}(z) = C_0 \left(\exp\left[-\frac{(z - z_c)^2}{2\sigma_z^2} \right] + \exp\left[-\frac{(z + z_c)^2}{2\sigma_z^2} \right] \right). \tag{3.1}$$

This is a representation of a mean concentration profile in the vertical direction at a particular downwind distance x, taking into account reflection of the plume from the ground, and ignoring the horizontal (y) variation in concentration. The plume spread about the plume centroid z_c is σ_z, and the maximum centreline value for the mean concentration in an unreflected plume is C_0.

The scripts used to process all the time series are contained under the `/scripts` directory, and are comprised of the files `rstats`, `stats.cfg`, `stats.pan` and `stats.mac`. These scripts produced the output files `*.txt` accompanying each binary data file. Final data analyses for each trial have been collected in Excel spreadsheets of the same name (with extension `.xls`), for which the `*.txt` files served as input. The spreadsheets contain all the uncertainty analysis and final results, together with any fitted profiles calculated.

Given the plume dispersion parameters C_0, σ_y and σ_z at fixed sampling lines downstream, the variation of these parameters with downwind distance x could be investigated. For a quantitative description, power law relationships varying as a function of x were fitted, and also compared with similar results for open terrain plume dispersion. Power laws generally fitted these downwind trends quite well, with acceptable χ^2 values. Gaussian plume profiles could not be fitted to oblique wind directions wd33 and wd49, so that σ_y and σ_z could not be derived for these types of releases. The profiles were too skewed to be well described by a Gaussian function, but the deviation of the maximum mean concentration from the plume centreline could be tracked as a function of downwind distance, showing evidence of street channelling of the dispersing material. The decay in maximum mean concentrations could also still be plotted and fitted with power law behaviour. Details of this analysis are contained in the directory `results/conc-stats/downwind-trends`.

3.5 Advanced Statistical Analysis

A considerable number of data files were also analysed in more detail for a variety of other advanced statistical descriptors, including power spectra, fitting of probability distributions, autocorrelation functions and integral time scales. A lot of technical details on the methods used will not be given in this report, but will be deferred to more detailed discussions in future papers, which will deal with comprehensive results and interpretation of the experiments. A brief summary of the analysis done is given below.

Processing scripts are available for all these analyses in the `/scripts` directory. All files of figures and processed data resulting from these analyses are contained in subdirectories given by the name of the original time series file, minus the `.bin` extension. In what follows, the time series file `ncb00ve2.bin` will be taken as an example to illustrate the organisation of all the subsequent data files. Thus the processed data files corresponding to the analysis of `ncb00ve2.bin` are all contained in the subdirectory `./ncb00ve2`.

Power spectra The power spectra analysis scripts are comprised of the files `rspec`, `spec.cfg`, `spec.pan` and `spec.mac`. It is possible to generate two types of output data files from these scripts, namely `ncb00ve2.spec` and `ncb00ve2.spec##`, where the `##` characters correspond to a two digit channel number `01`, `02`, ..., `11`, `12`. The `*.spec` files give all information for power spectra from one time series data file, including some header information, the frequencies that spectral values were

calculated for, and the actual power spectrum values for all channels. The `*.spec##` files were created to give a convenient two column data format listing frequency vs power spectral estimate for each individual channel, where the individual channel number is given by the characters `##`. This was useful for inclusion in other software plotting packages requiring such data input formats. The scripts can also generate PostScript plots of the power spectra, given by names such as `ncb00ve2-spec.ps`. Spectral estimates were formed by an inbuilt FAN routine, which used a standard method of dividing a time series up into M segments. Each segment was multiplied by a window function (usually a Welch window), then a periodogram estimate was made for each segment, and the final power spectrum estimate was formed by averaging over all the sub-periodograms (see [23]).

Probability distributions The fitting of probability distributions to the data was the most complex of all the analysis procedures performed. The clipped exponential, clipped normal and gamma distributions were investigated against cumulative distribution functions (CDFs) of the data, and fitted quantile vs data quantile plots. Probability density functions (PDFs) were also estimated by kernel smoothing techniques. Each channel in a time series data file has a collection of distribution data files and PostScript plots associated with it. Thus for example, for channel 3 in `ncb00ve2.bin`, there are the files

1.	`ncb00ve2-prob-ch03.hdr`	header file giving distribution parameters and file formats
2.	`ncb00ve2-ch03.cdf`	CDFs of data and fitted distributions
3.	`ncb00ve2-ch03.edf`	EDFs of data and fitted functions
4.	`ncb00ve2-ch03.pdf`	kernel smoothed PDF estimate
5.	`ncb00ve2-ch03.quan`	data quantiles and fitted quantiles
6.	`ncb00ve2-03cdf.ps`	plot of data CDF vs fitted CDFs
7.	`ncb00ve2-03edf.ps`	plot of data EDF vs fitted EDFs
8.	`ncb00ve2-03pdf.ps`	plot of kernel smoothed PDF estimate
9.	`ncb00ve2-03qa.ps`	plot of data quantiles vs fitted quantiles

The EDFs listed above are exceedance distribution functions; thus if $F(x)$ is a CDF, then $1 - F(x)$ is the corresponding EDF. EDFs plotted on logarithmic axes give a much better view of the closeness of a fitted distribution to the data near the right hand tail, where the actual probabilities are all very close to unity when viewed on a conventional CDF plot. The scripts and programs associated with the probability distribution analysis package include `rprob, prob.cfg, prob.pan, prob.mac, mkddir` (a small shell script) and `findphi` a compiled C++ program for calculating a certain parameter associated with the clipped normal distribution.

Autocorrelation functions and integral time scales The package comprised of the scripts `racorr, acorr.cfg, acorr.pan` and `acorr.mac` was used to calculate autocorrelation functions and concentration integral time scales. The data for autocorrelation functions calculated was not saved, though plots could also easily be generated. Of more interest is the actual integral time scales associated with these autocorrelation functions. A correlation time was taken as the time when the autocorrelation function first dropped to some fraction of its original value of unity (usually to 0.0, but other values are possible). This choice is rather arbitrary, as

analysis on other datasets has often used cutoff values of 0.1 or 0.05, depending on the noisiness of the data. The autocorrelation functions for the current trials tended to be quite smooth, with only very small lobes at large time lags, so that the low cutoff values were justified. This seems to be an indication of the stationary conditions achieved in the wind tunnel physical simulations. The correlation times extracted are always quite uncertain, due to the arbitrariness in the cutoff values and the oscillation of the autocorrelation function for large time lags (rather than uniformly decaying to zero). The integral time scales were then calculated by integrating the autocorrelation functions up to the correlation time cutoff. One data file by the name of `corr.txt` was saved for each set of trials (under the directories `day1, day2, day3, ...`). This file contained lists of correlation times and integral time scales for each set of time series analysed, together with the chosen cutoff for defining the correlation time (generally 0.0 or 0.05), and the lag interval used in integrating the autocorrelation function.

3.6 Velocity Statistics

Velocity time series were collected at locations shown in Figure 2.3 (pale blue plus symbol) at corresponding full-scale heights 2.5, 5, 7.5, 12.5, 20, 30, 40 and 50 metres. The crossed hotwire anemometers could measure two wind directions simultaneously, and time allowed for mainly only u-w measurements to be made, with just one u-v profile measured on the V6 tower. Mean wind profiles and turbulence intensity profiles for each wind component could easily be extracted from this data using the analysis scripts for statistics described earlier. Comparisons were made with standard atmospheric boundary layer similarity theory results of velocity statistics found in the literature (see e.g. [24]). Although, as explained earlier, no measurements could directly be made within the array canopy, the profile measurements could give some indication of the effect of the obstacle array on velocity statistics above it, as well as characterise in far greater detail the incoming flow profile. Velocity spectra for the different wind components were also calculated for many of the time series collected, using methods similar to that described above for the concentration spectra. These could be compared with various standard profiles of spectra often quoted in the literature, including neutral atmospheric spectra such as those derived by Kaimal [25], and idealised von Karman spectra for inferring turbulence length scales (see e.g. Panofsky and Dutton, page 197, [24]). This enabled an assessment to be made of how realistic the turbulence generated in the wind tunnel was in comparison to real atmospheric conditions. More details on these results with comparisons to standard open terrain results will be discussed in future papers.

4 Uncertainty Analysis

4.1 Overview

A careful consideration of the uncertainty in the results of data analysis is an aspect that usually receives little attention in wind tunnel and atmospheric dispersion experiments, despite a very rigorous approach to the subject in most branches of experimental

physics. This may be due to the intrinsic variability observed in the real atmosphere, where non-stationarity in the time series and appropriate interpretation pose the greatest challenge in data analysis. Given the fact that it is impossible to obtain repeated samples collected under identical conditions in the real atmosphere, it is very difficult to give an appraisal of the stochastic variability in the extracted statistics.

The wind tunnel provides a much more controlled environment, and it was deemed that an appraisal of the uncertainty attached to the results was a scientifically rigorous and complete approach to take. One obvious benefit would be a more meaningful comparison with full-scale MUST results, including an ability to single out aspects of wind tunnel model simulation that were failing to predict full-scale results correctly with a greater degree of confidence. Results reported with a full uncertainty appraisal will also be more useful to computational urban dispersion model validators, who wish to consider how closely their predicted results match with experiments. Thus an endeavour was made to consider the effects of the important factors contributing to the calculation of statistics, and weigh up the relative uncertainty of each. The methodology undertaken in this section is based on the current ISO recommendations [26].

The statistical quantity that was most influenced by experimental conditions was the dimensionless mean concentration

$$K = 60\frac{\overline{C}uL^2}{Q}. \tag{4.1}$$

This is not too surprising, given the range of experimental quantities from which it is constructed. We will decompose the variables in (4.1), in order to explicitly identify the various sources of experimental uncertainty.

The raw measurement of concentration consists of a voltage signal from a FID, which is stored as a number of a/d levels, 0, 1, ..., 4095. We first need to remove a/d level offset, by subtracting the integer 2048 from each sample in the time series, to produce a series of integers ranging from -2048 to 2047, which we will denote by $\{A_i\}_{i=1}^N$. The mean of this signal may be called A. We do not know the true baseline of $\{A_i\}_{i=1}^N$, so a baseline a/d level needs to be estimated. This leads us to the first contribution to uncertainty, with the others listed below:

Baseline uncertainty The procedure for estimating the baseline a/d level has been described in detail in Section 3.3. The "true" a/d level mean may thus be written as $A_t = A - B$, where B is the determined baseline a/d level for the channel in question. The value of B can typically be determined to within ± 1 a/d level. More details on particular levels of uncertainty used will be discussed below. Given the quantity A_t, the "true" mean voltage may be determined by $V = v_a A_t = v_a(A - B)$, with $v_a = 10000/2048$ being an *exact* conversion factor between a/d levels and voltage. Baseline uncertainty will be discussed in more detail in Section 4.2.

Calibration The mean voltage V must be converted to an actual concentration in ppm through a linear calibration constant k_i, via $\overline{C} = k_i V$ (for channel i). Calibration is a significant source of uncertainty, typically varying between 1–10% of the determined absolute value of the calibration constant. It will be discussed in detail in Section 4.3.

Intrinsic Variability For any practical experiment, a finite sampling time for time series collection imposes an inherent limitation on the accuracy to which statistics can be determined. Each statistic calculated is just one realisation from an infinite ensemble. Thus the statistics are just random variables of the stochastic process under investigation. Greater length of sampling leads to better convergence of statistics, but there are practical limitations. A detailed discussion of the methods used to assess the intrinsic stochastic variability in the calculated statistics is given in Section 4.5. This source of uncertainty was generally the largest of any of the contributions for the calculated statistics of most time series.

Reference Wind Speed A vane anemometer measured mean wind speeds at 1.0 m height for each 600 second trial period. This result was given as a digital read-out, always assumed accurate to ± 0.01 ms^{-1}.

Reference Length Scale The reference length scale selected was taken to be the height of the obstacles, $L = 48.4$ mm. The assumed accuracy was taken as ± 1.0 mm.

Source Flow Rate The source flow rate varied for various trials, in order to provide a reasonable strength signal at a given downwind distance of samplers. The gauge reading for the flow metre needed to be calibrated via a non-linear relationship. Thus given a gauge reading R in arbitrary units, the actual source rate Q (in cm^3/min) is given by the relation $R = aQ^2 + bQ$, with the predetermined calibration constants $a = 5.67 \times 10^{-5}$ and $b = 0.514$. The level of uncertainty in the gauge reading was assumed to be ± 50, which involved an uncertainty in accuracy of reading, and a tendency for the flow metre output to fluctuate to some extent. The uncertainty in a and b was considered negligible in comparison with this reading uncertainty.

In summary, we have a model of measurement for dimensionless mean concentration given by

$$K = 60 \times \frac{kv_a(A - B)uL^2}{Q}, \tag{4.2}$$

with the source rate given by

$$Q = \frac{1}{2a}\left(-b + \sqrt{b^2 + 4aR}\right). \tag{4.3}$$

The equation (4.2) is referred to as the model equation for the measurement, as it provides a mathematical model to translate actual physically measured data values into the "measured" quantity whose value we wish to estimate.

The other statistics are easier to deal with than the mean concentration. This is because they are all formed from ratios of moments, so that a lot of the experimental parameters cancel in their definitions. Apart from the uncertainty due to the ever-present intrinsic stochastic variability of the statistics, only the fluctuation intensity i_c has one other uncertainty contribution due to the baseline offset. The model equations of measurement for the other statistics corresponding to (4.2) are given by

$$i_c = \frac{\sigma_A}{A - B}, \tag{4.4}$$

$$s_c = \frac{\langle (A_i - A)^3 \rangle}{\sigma_A^3}, \tag{4.5}$$

$$k_c = \frac{\langle (A_i - A)^4 \rangle}{\sigma_A^4}, \tag{4.6}$$

where σ_A is the standard deviation of the time series $\{A_i\}_{i=1}^N$, and $\langle\,\rangle$ denotes averaging. Apart from the mean signal value contribution to i_c, which involves the baseline correction term, all terms in the above equations involve higher order moments of just the raw signal. The baseline correction term has cancelled out for all cases except in the mean signal value contribution to i_c (the $A - B$ term in the denominator of (4.4)). The experimentally determined parameters (such as u, L and Q) have also disappeared because of cancellations with ratios of moments. This then leaves only the stochastic variability as being a source of uncertainty in the calculation of s_c and k_c.

The following sections deal in more detail with methods for assessing the uncertainty due to each component listed above. The final uncertainty is given as a combination of the individual components of uncertainty

$$u_{\text{tot}}^2 = \sum_i (c_i u_i)^2, \tag{4.7}$$

where u_i is the standard uncertainty of the i-th contribution and c_i the corresponding sensitivity factor. The sensitivity factor is essentially a derivative of the model equation with respect to the variable whose uncertainty is under question. It thus serves as a constant that converts all contributions of uncertainty into a common system of units, namely the units of the measured quantity.

4.2 Baseline Uncertainty

The uncertainty in the baseline a/d level was one quantity that varied significantly with each channel recorded. In principle, it would have been possible to assign a fairly carefully considered (though still somewhat subjective to the data analyst) value of uncertainty for every channel collected, but this was ultimately deemed to be far too time consuming, and also of little value. The channels located in the centre of a plume tended to have strong signal output, and thus an error in the determined baseline level of even as much as one a/d level tended to be quite negligible. In considering the sum of uncertainty components given in (4.7) the baseline uncertainty contribution $(c_b u_b)^2$ was generally 2 to 3 orders of magnitude less than the contribution due to stochastic variability, $(c_s u_s)^2$. Hence the baseline uncertainty for these channels was always taken to be just one a/d level, which can be considered an absolute upper limit on the uncertainty for almost all the trials. Certain channels (particularly channel 8, which was usually in the bulk portion of a plume) tended to have poorer sensitivity (higher magnitude of calibration constant). For these channels, the relative importance of the baseline uncertainty tended to be greater, maybe 10 or 20% of the value of the uncertainty due to stochastic variability. This was also true for sampling lines further downstream (such as row AB). For these sampling lines, even using the maximum flow rate available from the source, the signal to noise ratio was lower due to greater dispersion downwind, and resulting reduction in mean concentration levels.

Consequently, the baseline contribution to the overall uncertainty tended to have a relative value of at least 10%.

More care was required in considering baseline uncertainties for channels near the edge of a plume. Here a highly intermittent signal and low signal to noise ratio made the mean concentration values calculated very sensitive to the value of the baseline level. Thus baseline levels generally needed to be specified to an absolute accuracy ranging from 0.01 to about 0.3 a/d levels, depending on the strength of signal and amount of noise and drift present in the baseline sections of the time series. For extreme cases, even an adjustment to the baseline level of 0.01 could mean the difference between a physically unrealistic negative or more plausible positive final mean concentration. These baseline values were able to be determined very accurately from the the long sections of zero concentration fluctuating baseline portions in the signals (interspersed only by several relatively large spikes). When some upper limits in the likely range of the baseline value for each channel were carefully determined, the relative contribution of the baseline uncertainty was usually kept somewhere between 1–10%. Only for some very intermittent channels with a very weak signal and possibly some baseline drift, were baseline uncertainty contributions comparable to those of the intrinsic stochastic variability of the statistics. Any absolute mean concentration values calculated for such channels had to be viewed with considerable scepticism in any case, and served more to just delineate the edges of a plume as being "close to zero concentration".

In the uncertainty calculations on the data spreadsheets, the baseline level uncertainty is represented by an absolute a/d level range $r_b = \pm 1$ a/d level for central plume channels, down to as low as $r_b = \pm 0.01$ a/d levels for the very edges of a plume. This range is taken to incorporate 100% of the possible range of values that the baseline level could possibly take, so that the degrees of freedom to be associated with the uncertainty contribution is $\nu_b = \infty$. The uncertainty contribution is obviously of Type B (in the ISO nomenclature [26]), and the distribution associated with this contribution will be taken to be triangular, with semi-range r_b. This gives a standard uncertainty of $u_b = r_b/\sqrt{6}$, and the sensitivity coefficient is given by

$$c_b = \left|\frac{\partial K}{\partial B}\right| = \frac{60 k_i v_a u L^2}{Q}.$$

4.3 Calibration Uncertainty

Calibration uncertainty is another significant Type B contribution, somewhat difficult to assess with much accuracy. The reason for this is that the value of the calibration constant could change slightly throughout the day, but generally only one calibration of the FIDs was done per day. To help guide the assessment of uncertainty better, an old set of calibrations from a previous set of trials was analysed, where two calibrations were done each day, one in the morning and one in the evening. The analysis for this set of calibrations is given in the spreadsheet `StadFidcal compare.xls`, under the directory `results/calibrations/StadCal`. A summary of this analysis is given here.

One trend that seemed apparent was that there was a tendency for the value of the calibration constant for each channel to increase in value between morning and evening calibrations (except for one channel – ch9 – which appeared to behave quite differently from

the others). Looking at the average percentage difference between evening and morning calibrations for each channel, the range was from $\Delta k = 1.6$–6.1%, with an overall average of $\Delta k = 4.7\%$ (ignoring ch9). Of course there was some scatter of percentage values for individual days, but the general trend was that for a significant number of channels, the hypothesis that there is no drift in the calibration constants over a day ($\Delta k = 0$) must be rejected at the 95% confidence level. On the other hand, the hypothesis that a drift in the calibration constants for each channel on average was consistent with $\Delta k = 4.7$ could be accepted for all channels except ch9.

The drift in calibration throughout a day is believed to be due to the nature of the FIDs, in particular how they require time to warm up (half an hour to an hour). To fully assess the nature of uncertainty of the FID calibrations, a repeated number of calibrations would need to be undertaken throughout a day. Such a study was impractical and outside the scope of the current trials. It is the belief of the wind tunnel operators that generally the FIDs' calibration constants change fairly rapidly in the first hour or two of operation, and then level off for the rest of the day. This would mean that the uncertainty due to calibration would be considerably lower than might otherwise be expected for most of the trials. We have however no concrete data to support this general belief.

The calibration constants of the FIDs change considerably from day to day for a variety of poorly understood reasons. Some effects probably are temperature changes, humidity, cleanliness of the long sampling filaments, and the very nature or precision to which each calibration was performed. By examining the percentage difference in calibration constants from one evening to the next morning, it was found that considerably more variation occurred. The standard deviation in the ensemble of percentage changes for each channel ranged from 3.4–13.0%, with an overall average standard deviation of 9.1%, compared with 4.8% for the average standard deviation of percentage differences in calibrations taken from morning to evening of the same day. The hypothesis that there was no definite trend in calibration constant differences from day to day however had to be accepted at the 95% confidence level. Thus as would be expected, calibration constants derived for each channel from day to day appeared to follow a random process, with a relatively high level of fluctuation. This is in contrast to the fact that there appeared to be a well-defined drift in values of the calibration constants determined at different times on the same day.

Another source of uncertainty in the values of the calibration constants is in the actual goodness-of-fit of the calibration curves to the measured points. This was not generally investigated for all the calibrations performed, but was considered in detail for Fidcal3 (see `results/calibrations/FIDCAL03.XLS`), which includes a regression analysis complete with uncertainty bounds. The calibrations were generally very linear over the range investigated, as can be seen by the value of the ratio of standard error to slope for each channel in Fidcal3, which lies around 0.02 for all cases.

Having taken all of the above into consideration, it seems pointless to try to come up with specific values of uncertainties in the calibrations for every single trial, given only one calibration run per day. There simply is not enough information available to justify the assignment of such values, and the process would also be very time consuming in the context of the complete data analysis effort of the trials. Ultimately, it was decided to choose a "reasonable" value for the uncertainty, given as a fixed percentage of the absolute value of the calibration constant for each channel. Given an average deviation in

the calibration constants for the various channels over a day of about 5%, it was decided to simply assign a standard uncertainty of $u_c = 5\%$ in the calibration constant. There is of course a scatter in values of calibration drift for individual channels about this mean value of drift, which as mentioned earlier was on average 4.8%, but this was then considered to average out over the entire set of experiments. The relatively small uncertainty in the actual goodness-of-fit for each calibration curve can be assumed to be absorbed into this 5% value. No doubt, for some of the days' trials the value of the calibration constant may have varied by more than 5%, but given the supposed stability in the FIDs' response when warmed up, a greater portion of the trials may well have (unknowable) uncertainties of less than 5%. This level of uncertainty seems like a reasonable compromise over the entire set of trials. It is also in keeping with the spirit of uncertainty estimation, whereby the value chosen should be a best estimate, rather than a very conservative bound.

In considering the relative importance of the calibration uncertainty contribution to the entire "sum-of-squares", Equ. (4.7), the magnitude of the calibration component $(c_c u_c)^2$ was generally an order of magnitude down from the stochastic uncertainty component $(c_s u_s)^2$ for sampling channels near the centre of the plume. Only for a couple of FID channels with poorer response (in particular ch8) did the contribution begin to approach the level of $(c_s u_s)^2$. This gives some further retrospective support to the very general selection of a 5% level of uncertainty in the calibration constants.

In the uncertainty calculations on the data spreadsheets, the standard calibration uncertainty is given in ppm/mV as simply 5% of the value of the calibration constant k_i for channel i. The assumed distribution for the contribution is normal. Given the very approximate nature of the assignment of 5% uncertainty, the relative uncertainty in the confidence of this assignment is very high. Thus only 2 degrees of freedom, $\nu_c = 2$ have been assumed as a measure of confidence in the chosen value. The sensitivity factor is given by $c_c = K/k_i$.

4.4 Other Contributions of Uncertainty

Before we tackle the difficult subject of the intrinsic stochastic contribution to the uncertainty estimates, we discuss the remaining sources of uncertainty, which are simple to deal with. They remain invariant over all the trials. Their contribution to the overall uncertainty of results is always small. The consistent and simple nature of the calculations involved made the contributions easy to include in all the spreadsheet calculations of uncertainty, though they generally had a small influcence in the final results.

The *reference wind speed* uncertainty (Type B) has a semi-range of $r_u = 0.01\text{ms}^{-1}$ and will be assumed to be modelled by a rectangular distribution, due to the digital nature of the reading. Then the standard uncertainty $u_u = r_u/\sqrt{3}$. The relative uncertainty associated with the limits of this distribution will be assumed to be 50%, giving just $\nu_u = 2$ degrees of freedom. The sensitivity coefficient is given by $c_u = K/u$.

The *reference length scale* uncertainty (Type B) has a semi-range of $r_l = 1.0$ mm and will be assumed to be modelled by a triangular distribution. Then the standard uncertainty $u_l = r_l/\sqrt{6}$. The bounds of this distribution are considered certain, giving $\nu_l = \infty$ degrees of freedom. The sensitivity coefficient is given by $c_l = 2K/L$.

The value of the *source flow rate* appears in the definition of K (Equ. (4.1)) in a nonlinear fashion through the calibration curve $R = aQ^2 + bQ$. However, given the relative value of the calibration constants a and b, the dependence is still approximately linear, and the contribution to uncertainty can be included in the usual sum-of-squares equation (4.7) (rather than the inclusion of some higher order nonlinear terms). The assumed semi-range of the uncertainty is $r_r = 50$ (given in arbitrary gauge units), and will be considered to be modelled by a triangular distribution. Then the standard uncertainty $u_r = r_r/\sqrt{6}$. The relative uncertainty associated with the limits of this distribution will be assumed to be 10%, giving $\nu_r = 50$ degrees of freedom. Due to the slight nonlinearities, the sensitivity coefficient for the source flow rate uncertainty is more complicated. It is given by the expression

$$c_r = \frac{K}{Q}\frac{1}{2aQ + b}$$

.

4.5 Stochastic Uncertainty

One of the inherent problems with atmospheric dispersion experiments is the difficulty in actually achieving a stationary stochastic process. In outdoor trials, obtaining a truly stationary process is impossible, because of the ever-changing direction of the mean wind from mesoscale and larger–scale forcings, as well as slow changes in other ambient environmental variables. The very question of what constitutes a mean quantity is somewhat open, as different results will be obtained for different averaging times.

In a wind tunnel, the mean wind direction is far easier to control, but the inherent turbulence within the flow means that finding the "true" mean concentration over a given time interval is still not trivial. The spectrum of atmospheric turbulence shows ever larger scales of eddies at the low frequency end, until some unnatural cutoff point is reached, due to the finite instrumental sampling time, or some other artificial effect. In the wind tunnel, this cutoff corresponds to the width and height of the tunnel, as this is the maximum scale of eddies that can be accommodated. To achieve statistically converged results from the time series, the sampling period needs to be long enough to sample a great enough number of the largest scale eddies. The optimum sampling time can only really be worked out by trial and error. It is possible to sample for an extremely long time, but the extra accuracy gained for each extension of the sampling period gradually improves more and more slowly to a practical upper limit. For example, given that the statistics calculated for 600 seconds samples proved to be accurate to within about 10%, increasing the sampling time to 1200 seconds may well only improve this accuracy an extra percent or two. With experimental time limited by the project budget, this would ultimately be to the detriment of the experimental scope, as far fewer configurations would have been able to be tested.

From prior experience with the Monash University wind tunnel, it was known that a sampling time of 5–10 minutes was appropriate. A number of repeated trials were initially undertaken in an attempt to gauge the difference between 5 and 10 minute sampling times. These were trials with wd00, release type B (midpoint between containers K5 and L5), in the first sampling line, row IJ (data files `ncb00ij*`). Time series were collected first for three identical configurations (`ncb00ij2`, `ncb00ij4` and `ncb00ij5`), and then the wind speed and release rate were also varied for trials `ncb00ij1`, `ncb00ij3` and `ncb00ij6`. This

Channel Number	Transverse Position y/H	$\sigma_K/\langle K \rangle$ 600 sec	300 sec
2	-20.95	0.59	0.71
3	-16.76	0.22	0.32
4	-8.38	0.23	0.25
6	-4.19	0.10	0.12
7	0.00	0.09	0.09
8	4.19	0.13	0.14
9	8.38	0.13	0.17
10	12.57	0.21	0.29

Table 4.1: Comparison of the statistical convergence of mean concentration for 300 second and 600 second time series samples. The listed values are the ratios of the sample standard deviation to sample mean of the ensemble of mean concentrations obtained.

enabled any significant variation in the theoretically constant dimensionless mean concentration K to be detected, by varying its defining parameters. By looking at the dimensionless mean concentration for the various runs, greater variation in the trials `ncb00ij1`, `ncb00ij3` and `ncb00ij6` than in the identical repeats would indicate a departure from the assumed scaling relations. Fortunately such a departure did not seem evident from the data. For a more complete statistical analysis, a larger number of samples would have been preferable, but time constraints limited the number of repeated trials that could be done. The collection of 300 second samples were obtained by simply dividing the 600 second time series in half, to give twice as many samples in the ensemble. The individual 300 second samples are assumed to be fairly statistically independent in their lower statistical moments, even though they have been obtained by cutting up a longer time series, since the autocorrelation times of the time series are quite short (5 seconds or less). The mean $\langle K \rangle$ and standard deviation σ_K of the ensemble were then calculated for each channel, and a ratio of $\sigma_K/\langle K \rangle$ was used to provide a measure of the stochastic variability of each channel under the given sampling time. A small ratio implied a small spread of results in relation to the absolute value of the mean concentration measurement. A brief excerpt from the calculation is given in Table 4.1. The complete analysis is given in the spreadsheet file `Kvar_ncb00ij.xls` under the directory `results/conc-stats/row-ij/`.

It should be noted that the results in the table are fairly rough, as the calculations were done in the initial stages of the experiments, before careful baseline corrections had been applied to the time series (though some initial corrections had been applied using the real time analysis scripts developed). Other experimental uncertainties are also not taken into account. It is obvious that statistical convergence deteriorates further from the plume centreline. This is to be expected, given the much greater intermittency of the time series at the edges of plumes. A greater number of the intermittent spikes in concentration or eddy turnover times would need to be sampled to achieve better statistical convergence, i.e. a much larger sampling time would be required.

The preliminary results of Table 4.1 indicate that a little extra convergence of statistics is gained by using 600 second sampling times, but that the improvement is not very significant. Some higher order statistics gained a little more accuracy from the 600 second sampling time. Ultimately a 600 second time was chosen as the standard, taking into

consideration other aspects of data analysis as well. The other aspects included the ability to produce better resolution or smoother concentration power spectra from the longer sampling times, the better fitting of theoretical probability distributions to the data, and the calculation of smoother PDFs.

Another set of repeated trials was done for the configuration `ncb00gh*`. Only 4 runs were done under this set, with two being identical (same wind speed and source flow rate), and then wind speed and source flow rate being varied. This set of repeats also supported the scaling hypothesis in the dimensionless concentration K, and the variation over 600 second samples seemed similar to the results given above. Detailed calculations for the 600 second averaged mean concentrations are given in the spreadsheet `ncb00gh-mean.xls` under the directory `/results/conc-stats/row-gh/`. Due to the completeness of this ensemble in correctly functioning FIDs in comparison to the 6 repeats `ncb00ij*`, analysis for a wide variety of sample lengths was also done (60, 90, 120, 240, 300 second lengths). As well as to give an indication of the stochastic variability in an ensemble, this analysis was also used to test the sensitivity of Gaussian plume parameters to sampling time (discussed in detail in a future paper). The results of this analysis are given in the spreadsheet `ncb00gh-compare.xls`. The stochastic variability contribution to overall uncertainty was of a statistical nature (type A), in contrast to all other type B components of uncertainty. The final assessment of the magnitude of the stochastic uncertainty is not entirely trivial, and requires some theoretical development. This discussion, which is more mathematically technical in nature, is given in Appendix A.

To summarise the findings of Appendix A, we need to consider a collection of n repeated measurements y_i of a physical quantity Y, each of which has been calculated as a certain statistic of a particular time series in a collection of n time series. Each y_i will have attached to it an instrumental (Type B) uncertainty u_i, which may be considered an aggregate of all the other uncertainty contributions listed in Section 4.1. It is shown in Appendix A that an estimate for the underlying "true" Type B uncertainty σ_ϵ^2 is given by the equation

$$\hat{\sigma}_\epsilon^2 \equiv \frac{1}{n}\sum_{i=1}^{n} u_i^2, \tag{4.8}$$

with the caret ($\hat{}$) denoting a statistical estimator. It is then shown that a statistical estimator for the intrinsic stochastic uncertainty $u_s \equiv \sigma_\tau$ may be formed by the difference between the simple variance of the collection of measurements $\hat{\sigma}_Y^2$ and the estimate of Type B uncertainty given by (4.8), namely

$$\begin{aligned} \hat{\sigma}_\tau^2 &\equiv \hat{\sigma}_Y^2 - \hat{\sigma}_\epsilon^2 \\ &= \frac{1}{n-1}\sum_{i=1}^{n}\left(y_i - \bar{Y}\right)^2 - \frac{1}{n}\sum_{i=1}^{n} u_i^2. \end{aligned} \tag{4.9}$$

Given the results (4.8) and (4.9), the stochastic uncertainty associated with the trials may finally be estimated from the set of repeated runs `ncb00ij` and `ncb00gh`. Some practical considerations must first be highlighted. In theory, the overall experimental variance σ_Y^2 is always greater than the instrumental Type B uncertainty σ_ϵ^2. In practice however, with small sample sizes, the estimates for these quantities may not always follow this relationship, so that the difference in variances given in (4.9) may sometimes be negative.

It turned out that this never happened for the set of runs `ncb00ij` (with 6 repeats), but did in a couple of channels for `ncb00gh` (with 4 repeats). The reason for this is that by coincidence, for this random sample, the experimentally determined values happened to all be very similar, giving a smaller than might "usually" be expected sample variance (an occurrence which would be far less likely for a larger sample). Results from these channels had to be ignored, as they gave non-sensical information about the stochastic uncertainties.

The final analysis for the repeated runs is given in the spreadsheets `ncb00ij-mean.xls` and `ncb00gh-mean.xls` for the mean dimensionless concentrations, and in the spreadsheets `ncb00ij-flamp.xls` and `ncb00gh-flamp.xls` for the concentration fluctuation intensities. Skewness and kurtosis for these repeated sets of trials were also considered in `ncb00ij-skew-kurt.xls` and `ncb00gh-skew-kurt.xls`, and were much easier to analyse, because stochastic uncertainty formed the only contribution for these statistics. The uncertainties in the experimentally determined quantities becomes higher towards the channels at the edge of the plumes, due to the greater intermittency and weaker signals detected there. Ultimately, some overall generic stochastic uncertainties were proposed, taking into account all the repeated trials. Such uncertainties necessarily depended on the position of the samplers relative to the centre of the plume. Obviously, with small ensembles of repeated runs, variation could be expected across similar groups of channels.

For some pre-defined groups of channels, generic uncertainty values were determined for all trials, by considering ratios of standard uncertainties with measured quantities. Thus, given a collection of concentration statistics y_i (which may be a collection of measured values of K, i_c, s_c or k_c) calculated for a group of channels (with each index i corresponding to one of the channels in the group), a set of standard uncertainties for the stochastic variability u_{si} could be determined for each measured concentration statistic. The average value $\bar{u}_s$ of the ratio u_{si}/y_i (the stochastic uncertainty of each channel relative to the mean) was formed for the group of channels. This value was then simply converted into a percentage for the group of channels, thus

$$\bar{u}_s = \left\langle \frac{u_{si}}{y_i} \right\rangle \times 100\%. \tag{4.10}$$

The groups ultimately were divided into central plume channels, channels closer to the edge of the plume, and extreme plume edge channels. Thus uncertainties were assigned as a percentage of the value of the measured quantity, given a particular position of the sampler within the plume (e.g. for a mean dimensionless concentration K measured near the plume centreline, the stochastic uncertainty u_s may be given by $u_s = 10\% \times K$).

A final guideline for percentage uncertainties applied to each concentration statistic, given the grouping of channels according to position in the plume, is given in the spreadsheet `results/conc-stats/Intrinsic-unc.xls`. The percentage uncertainty values given in `Intrinsic-unc.xls` were not applied automatically for every channel in every trial. At times, given the distance downstream of the sampling line, the shape of the plume, and the spacing of the samplers within a line, some judgement had to be made of the correct value of uncertainty to apply, keeping the guidelines in mind.

The assignment of the stochastic uncertainties was inherently subjective, but did represent the best estimates available from the given data. Ideally, a set of repeated trials

for each sampling line would have been welcome, but was experimentally too expensive. There is some suspicion that the uncertainty levels applied from the repeated trials was too high for sampling lines further downstream of the source. This is due to the extremely good fit of Gaussian curves (given by very low χ^2–values) to the mean concentration data in these sampling lines—better than may be expected from usual experimental variability. Greater mixing and less meandering of the plume further downstream may account for a reduction in uncertainty, which was not able to be determined from the set of repeated runs done by sampling lines in rows IJ and GH (relatively close to the source).

The Type A stochastic uncertainty components had an assumed Gaussian distribution, and the percentage value of uncertainty u_y, given in (4.10), assigned for each channel was taken to be the standard uncertainty value u_i given in (4.7). Assignment of a relative uncertainty in the estimates of the generic standard uncertainty was fairly arbitrary from the limited data. A value was arrived at by considering the standard deviation Δu_s in the collection of ratios for each group of channels u_{si}/y_i discussed above. This standard deviation was then compared to the average of the ratios u_s (which was the actual standard uncertainty for the group of channels), so that the ratio $\Delta u_s/u_s$ gave the relative uncertainty in the standard uncertainty estimate. For example, consider the mean concentration K of a central plume channel that has a stochastic uncertainty of 10%, $u_s = 0.1K$. The standard deviation in the collection of values of u_{si}/K_i for each channel in the central group was $\Delta u_s/u_s = 0.36$. Then the relative uncertainty in u_s was assigned approximately as 35% (reducing the estimate 0.36 to a "round number"), which corresponds to 4 degrees of freedom.

5 Conclusions and Further Work

This report has described in considerable detail the experimental setup, procedure and data analysis methods used in the MUST wind tunnel simulations. The types of analysis covered has included basic statistics derived from both concentration and velocity time series, power spectra, autocorrelation functions, integral time scales, kernel smoothed PDF estimates, and fitting of theoretical distributions to the data through CDF and fitted vs data quantile plots. Particular emphasis has been placed on the uncertainty attributable to calculated quantities. This has required careful consideration of the intrinsic stochastic variability of the experimentally determined quantities, caused by the finite sampling time of an ostensibly stationary stochastic process. Estimation of this variability has relied on a small set of repeated trials, and a carefully thought out application of statistical and probability theory to separate out the uncontrollable Type B experimental uncertainties with the statistical Type A uncertainty. Attempts have been made to give best estimates of all the major Type B experimental uncertainties, without going into excessive painstaking analysis for every individual trial and attributing very precise sources of uncertainty where they cannot be reasonably justified. Such an approach is illustrated with the general type of assumptions made on the magnitude of uncertainty for the calibration and baseline corrections. Calculation of the uncertainty in the mean concentrations has required the most effort in this analysis, and this is probably well-justified, due to the importance normally attached to the mean concentration values in dispersion modelling, both in theory and in practice. It has also served the advantage in the current investigations of attributing

very realistic values of uncertainty to individual data points when attempting to fit curves (particularly Gaussian profiles and power law dependencies) to the mean concentration values, thus giving informative χ^2 measures of the fitted results.

It has been found in general that the stochastic variability attributable to a finite sampling time generally provides the greatest source of uncertainty in the various calculated statistics, and that sampling for longer time periods would not provide any significant gains in accuracy obtainable. For certain channels with a large value of calibration constant, and for some channels near the edges of a plume, uncertainty in the calibration constants and baseline corrections respectively did at times prove to provide significant sources of uncertainty. Other physical parameters with which an uncertainty source was easy to identify generally were quite negligible in comparison.

With the very carefully laid out methodology of the current trials, and a powerful set of well-documented data analysis scripts now in mature development, it is anticipated that future wind tunnel experiments of a similar nature will lend themselves to quick and insightful analysis.

Further reporting on the MUST experiments is now called for, and will be dealt with in separate papers. In particular, a detailed description of all the results of the wind tunnel simulations will be collected in a companion paper, to give a very comprehensive picture of the underlying physical processes responsible for plume dispersion within this obstacle array. Of even greater value will be a paper currently under preparation, which seeks to compare the water channel and full-scale experiments with these wind tunnel simulations. Such a comparative study will highlight any differences in the physical modelling at different scales, using different instrumentation, and in differing dispersive media, giving an unprecedented understanding of the mechanisms of plume dispersion in obstacle arrays, and the limitations of physical modelling.

References

1. Pasquill, F. (1983) *Atmospheric Diffusion*, John Wiley & Sons, New York, USA.
2. Meroney, R. N. (1982) Turbulent diffusion near buildings, *in* E. J. Plate, ed., *Engineering Meteorology*, Elsevier, Amsterdam, chapter 8, pp. 481–525.
3. Hosker, R. P. (1984) Flow and diffusion near obstacles, *in* D. Randerson, ed., *Atmospheric Science and Power Production*, number 3, Technical Information Center, U.S. Department of Energy, Washington D.C., chapter 7, pp. 241–326.
4. Hosker, R. P. (1985) Flow around isolated structures and building clusters: A review, *ASHRAE Transactions* **21(2B)**, 1671–1692.
5. Davidson, M. J., Mylne, K. R., Jones, C. D., Phillips, J. C., Perkins, R. P., Fung, J. C. H. & Hunt, J. C. R. (1995) Plume dispersion through large groups of obstacles—a field investigation, *Atmospheric Environment* **29**, 3245–3256.
6. Davidson, M. J., Snyder, W. H., Jr., R. E. L. & Hunt, J. C. R. (1996) Wind tunnel simulations of plume dispersion through groups of obstacles, *Atmospheric Environment* **30**, 3715–3731.
7. Macdonald, R. W., Griffiths, R. F. & Cheah, S. C. (1997) Field experiments of dispersion through regular arrays of cubic structures, *Atmospheric Environment* **31**, 783–795.
8. Macdonald, R. W., Griffiths, R. F. & Hall, D. J. (1998) A comparison of results from scaled field and wind tunnel modeling of dispersion in arrays of obstacles, *Atmospheric Environment* **32**, 3845–3862.
9. Hall, D. J., Macdonald, R., Walker, S. & Spanton, A. M. (1996) *Measurements of Dispersion Within Simulated Urban Arrays—a Small Scale Wind Tunnel Study*, Client Report CR 178/96, Building Research Establishment Ltd., Garston, Watford, UK.
10. Hall, D. J., Spanton, A. M., Macdonald, R. & Walker, S. (1997) *A Simple Model for Estimating Dispersion in Urban Areas*, Client Report CR 169/97, Building Research Establishment Ltd., Garston, Watford, UK.
11. Biltoft, C. A. (2001) *Customer Report for Mock Urban Setting Test*, Technical Report WDTC-FR-01-121, U.S. Army Dugway Proving Ground, Dugway, Utah.
12. Biltoft, C. A., Yee, E. & Jones, C. D. (2002) Overview of the Mock Urban Setting Test, *in Fourth Symposium on the Urban Environment*, American Meteorological Society, Norfolk, Virginia, USA.
13. Yee, E. & Biltoft, C. A. (2002) Preliminary results of the MUST diffusion experiment, *in Fourth Symposium on the Urban Environment*, American Meteorological Society, Norfolk, Virginia, USA.
14. Yee, E. & Biltoft, C. A. (2002) On the structure of plumes dispersing through a large array of obstacles, *in* S. Hanna, ed., *Sixth Annual George Mason University Transport and Dispersion Modeling Workshop*, Defense Threat Reduction Agency, Fairfax, Virginia.
15. Yee, E. & Biltoft, C. A. (2004) Concentration fluctuation measurements in a plume dispersing through a regular array of obstacles, *Boundary-Layer Meteorology* **111**, 363–415.

16. Gailis, R. M. & Yee, E. (2002) Wind tunnel simulations of the mock urban setting test at dugway, *in* S. Hanna, ed., *Sixth Annual George Mason University Transport and Dispersion Modeling Workshop*, Defense Threat Reduction Agency, Fairfax, Virginia.

17. Melbourne, W. H., Taylor, T. J. & Grainger, C. F. (1994) Dispersion modelling in convective wind flows, *Atmospheric Environment* **28**(11), 1879–1885.

18. Meroney, R. N. & Melbourne, W. H. (1992) Operating ranges of meteorological wind tunnels for the simulation of convective boundary layer phenomena, *Boundary–Layer Meteorology* **61**, 145–174.

19. Standards Association of Australia (1989) *AS 1170.2-1989 Minimum Design Loads on Structures (known as the SAA Loading Code)—Wind Loads*, fifth edn, North Sydney.

20. Deaves, D. M. & Harris, R. I. (1978) *A Mathematical Model of the Structure of Strong Winds*, Technical Report 76, Construction Industry Research and Information Association (U.K.).

21. Stull, R. B. (1988) *An Introduction to Boundary Layer Meteorology*, Kluwer, Dordrecht, The Netherlands.

22. Kosteniuk, P. (1996) *FAN Version 2.30 User's Manual*, Kosteniuk Consulting Ltd., 429 6th Street East, Saskatoon, Saskatchewan, Canada.
email: kostp@shaw.ca.

23. Press, W. H., Teukolsky, S. A., Vetterling, W. T. & Flannery, B. P. (1996) *Numerical Recipes in C: The Art of Scientific Computing*, second edn, Cambridge University Press, Cambridge, UK.

24. Panofsky, H. A. & Dutton, J. A. (1984) *Atmospheric Turbulence, Models and Methods for Engineering Applications*, John Wiley & Sons, New York, USA.

25. Kaimal, J. & Finnigin, J. (1994) *Atmospheric Boundary Layer Flows—Their Structure and Measurement*, Oxford University Press, Oxford, UK.

26. International Organisation for Standardisation (ISO) (1995) *Guide to the Expression of Uncertainty in Measurement*, Geneva, Switzerland.

Appendix A Theoretical Developments in Uncertainty Assessment

To give a final estimate of the stochastic variability of the various calculated statistics under a given sampling time, this intrinsic variability has to be separated out from the non-statistical (Type B) sources of uncertainty. This requires the correct interpretation of the standard deviations of the measurements in the ensembles of repeated trials that were collected. Here we give a theoretical motivation for the method chosen to estimate the stochastic variability, which to our knowledge is an original development.

Consider first a single experimentally determined observation y_i of a physical quantity Y, which will be assumed to be calculable as a statistic of some collected time series (such as the dimensionless mean concentration). The final measured value can be decomposed into three contributions:

$$y_i = \mu + \tau_i + \epsilon_i. \tag{A1}$$

The final value y_i is the only actual value that can be measured, and the various contributions have to be estimated from statistical and uncertainty theory. The "true mean" μ, whose precise value is unknowable, is the real quantity of interest that we desire to estimate, being a particular experimentally determined value of Y. It is the one underlying quantity that does not change with every individual observation, and may thus be estimated by statistical methods. Given the stochastic nature of the underlying physical process, any realisation of the quantity Y is subject to stochastic variability for finite sampling time, whose fluctuating contribution is given by τ_i. By the definition of a stochastic variation about some mean, the expectation of τ_i must be zero, but it is expected to have a finite dispersion, the same for each individual measurement:

$$E[\tau_i] = 0, \qquad V[\tau_i] = \sigma_{\tau_i}^2 \equiv \sigma_\tau^2, \tag{A2}$$

for all i, where $E[\ ]$ is the expectation operator, and $V[\ ]$ the variance operator. As discussed earlier, we expect $\sigma_\tau \to 0$, or complete convergence of the measured samples to the "true value" (assuming no experimental imprecision), as the sampling time becomes infinite (a condition of ergodicity). Finally there is the experimental uncertainty from the other Type B sources (uncertainty due to instrumentation), described in detail in Section 4, given by ϵ_i. This quantity too has a fluctuating value about some zero expectation:

$$E[\epsilon_i] = 0, \qquad V[\epsilon_i] = \sigma_{\epsilon_i}^2 \equiv \sigma_\epsilon^2. \tag{A3}$$

Given the specification of the moments of the contributing random sources in (A2) and (A3), a similar statement may be made about the observable quantity, namely

$$E[y_i] = \mu, \qquad V[y_i] = \sigma_Y^2 = \sigma_\tau^2 + \sigma_\epsilon^2. \tag{A4}$$

This follows from the fact that the random variables τ_i and ϵ_i are statistically independent. The relationship between the various random variables constituting the physical process is illustrated schematically in Figure A1.

Consider now a sample of n observations $\{y_i\}_{i=1}^n$, each with an experimentally determined uncertainty $u_i = \hat{\sigma}_{\epsilon_i}$. (Symbols with a caret will denote statistical estimators of a

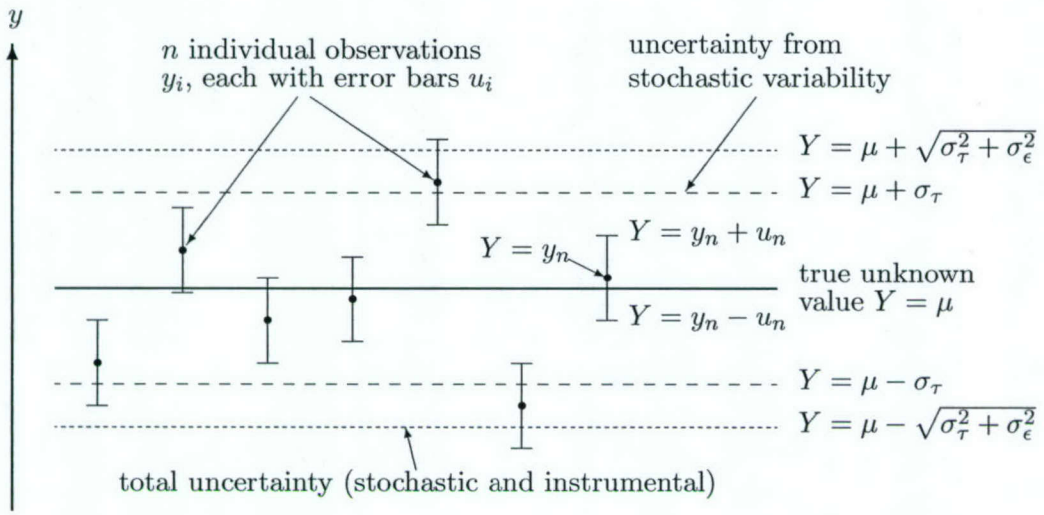

Figure A1: Illustrative relationship between the total uncertainty in a physical parameter, the individual measurements, and the constituting components of uncertainty.

theoretical parameter.) The u_i are estimators for the standard deviation of the true uncertainty σ_ϵ, which cannot be precisely determined (as we do not have unlimited information about the physical system under investigation). We define the sample mean and variance

$$\hat{\mu} \equiv \bar{Y} = \frac{1}{n}\sum_{i=1}^{n} y_i, \tag{A5}$$

$$\hat{\sigma}_Y^2 \equiv s_Y^2 = \frac{1}{n-1}\sum_{i=1}^{n} \left(y_i - \bar{Y}\right)^2. \tag{A6}$$

The sample mean of the measurements $\bar{Y}$ gives an experimentally determined estimate of μ. We wish to explore the significance of the sample variance s_Y^2 to uncertainty theory. These quantities, derived from statistical sampling theory, need to be related to the postulated underlying random variables of the measurement process, in particular the variances σ_ϵ^2 and σ_τ^2. To proceed, we expand the expression for s_Y^2 in terms of its constituent parts by substituting (A1). The following representation is obtained:

$$\begin{aligned}\sum_{i=1}^{n} \left(y_i - \bar{Y}\right)^2 &= \sum_{i=1}^{n} \left(\mu - \bar{Y}\right)^2 + \sum_{i=1}^{n} \tau_i^2 + \sum_{i=1}^{n} \epsilon_i^2 \\ &\quad + 2\sum_{i=1}^{n} \left[\epsilon_i(\mu - \bar{Y}) + \tau_i(\mu - \bar{Y}) + \tau_i\epsilon_i\right].\end{aligned} \tag{A7}$$

We now take the expectation of this equation, which should yield an estimate for the underlying variance or uncertainty in the measured physical quantity. Recognising the expectation values of the various quantities given by (A2) and (A3), and the fact that τ_i and ϵ_i are statistically independent (which leaves the last term zero in the expression above), the final expression

$$E\left[\sum_{i=1}^{n} \left(y_i - \bar{Y}\right)^2\right] = E\left[n\left(\mu - \bar{Y}\right)^2\right] + E\left[\sum_{i=1}^{n} \tau_i^2\right] + E\left[\sum_{i=1}^{n} \epsilon_i^2\right] \tag{A8}$$

is obtained.

The first term on the right-hand-side of (A8), namely

$$E\left[n\left(\mu-\bar{Y}\right)^2\right] = nE\left[\bar{Y}^2\right] - n\mu^2, \tag{A9}$$

needs more attention. We must consider in detail the expansion of the quantity

$$E\left[\bar{Y}^2\right] = \frac{1}{n^2}E\left[\left(\sum_{i=1}^{n}(\mu+\tau_i+\epsilon_i)\right)^2\right]. \tag{A10}$$

After considerable algebraic manipulation, it may be shown that

$$E\left[\bar{Y}^2\right] = \frac{1}{n^2}\left(n^2\mu^2 + E\left[\sum_{i=1}^{n}\tau_i^2\right] + E\left[\sum_{i=1}^{n}\epsilon_i^2\right]\right). \tag{A11}$$

This expanded result for $E[\bar{Y}^2]$ may be combined with Equs. (A8) and (A9) to obtain a final expansion for $E[s_Y^2]$:

$$E\left[s_Y^2\right] = \frac{n+1}{n(n-1)}E\left[\sum_{i=1}^{n}\tau_i^2\right] + \frac{n+1}{n(n-1)}E\left[\sum_{i=1}^{n}\epsilon_i^2\right]. \tag{A12}$$

This equation gives an estimator for the overall variance of the measured physical quantity Y. This can be seen from the definition

$$\sigma_Y^2 \equiv E\left[\hat{\sigma}_Y^2\right] \equiv E\left[s_Y^2\right].$$

It now remains to attach some experimentally determined quantities to the theoretical expressions on the right-hand-side of (A12). From (A4), $\sigma_Y^2 = \sigma_\tau^2 + \sigma_\epsilon^2$, thus we deduce that

$$\begin{aligned}
\sigma_\tau^2 &= \frac{n+1}{n(n-1)}E\left[\sum_{i=1}^{n}\tau_i^2\right], \quad \text{so define} \quad \hat{\sigma}_\tau^2 \equiv \frac{n+1}{n(n-1)}\sum_{i=1}^{n}\tau_i^2, \\
\sigma_\epsilon^2 &= \frac{n+1}{n(n-1)}E\left[\sum_{i=1}^{n}\epsilon_i^2\right], \quad \text{so define} \quad \hat{\sigma}_\epsilon^2 \equiv \frac{n+1}{n(n-1)}\sum_{i=1}^{n}\epsilon_i^2.
\end{aligned}$$

These expressions give estimators for σ_τ^2 and σ_ϵ^2 as the expectations of sums of squared random variables, however these random variables τ_i and ϵ_i cannot be directly determined, but only estimated through experimental methods. Consequently we form the estimates in terms of the ensemble of measured values $\{y_i\}_{i=1}^n$ and the corresponding estimated uncertainties u_i:

$$\hat{\sigma}_\epsilon^2 \equiv \frac{1}{n}\sum_{i=1}^{n}u_i^2, \tag{A13}$$

$$\begin{aligned}
\hat{\sigma}_\tau^2 &\equiv \hat{\sigma}_Y^2 - \hat{\sigma}_\epsilon^2 \\
&= \frac{1}{n-1}\sum_{i=1}^{n}\left(y_i-\bar{Y}\right)^2 - \frac{1}{n}\sum_{i=1}^{n}u_i^2.
\end{aligned} \tag{A14}$$

Thus the implied overall uncertainty of instrumental errors has been estimated as the average of the Type B uncertainties for each observation (A13). Furthermore, a method has

been established for estimating the intrinsic stochastic variability σ_τ^2 as the difference of the variance of the ensemble of observations with this estimated average Type B uncertainty (A14).

We have now established a general method to calculate estimates for the stochastic variability given an ensemble of measurements, which when applied to the sets of repeated runs (i.e. `ncb00ij*` and `ncb00gh*`) can be used to estimate the stochastic variability for the entire set of trials. We would also like to find the actual uncertainty of an experimentally determined variable from one ensemble of measurements (e.g. what is the uncertainty in K for a given channel, given the set of trials `ncb00ij*`?). This involves attaching a final uncertainty estimate $\hat{\sigma}_{\bar{y}}$ to the mean of the ensemble of measurements taken. Thus we need to consider the uncertainty on the unbiased estimate $\hat{\mu} \equiv \bar{Y}$ of μ. This is given by the standard variance relationship

$$\begin{aligned} \sigma_{\bar{Y}}^2 \equiv V[\bar{y}] &= \frac{1}{n^2} V\left[\sum_{i=1}^{n} \tau_i\right] + \frac{1}{n^2} V\left[\sum_{i=1}^{n} \epsilon_i\right], \\ &= \frac{1}{n^2} \sum_{i=1}^{n} \sigma_{\tau_i}^2 + \frac{1}{n^2} \sum_{i=1}^{n} \sigma_{\epsilon_i}^2, \end{aligned} \tag{A15}$$

since all the random variables are independent. Now since the measurements are assumed to involve a stationary stochastic process, the $\sigma_{\tau_i}^2$ and $\sigma_{\epsilon_i}^2$ are all equal, and the result

$$\sigma_{\bar{Y}}^2 = \frac{\sigma_\tau^2}{n} + \frac{\sigma_\epsilon^2}{n} \tag{A16}$$

follows. The estimates for σ_τ^2 and σ_ϵ^2 are given in Equs. (A13) and (A14), so that the simple relation

$$\hat{\sigma}_{\bar{Y}}^2 = \frac{1}{n(n-1)} \sum_{i=1}^{n} (y_i - \bar{Y})^2 \tag{A17}$$

is finally obtained. Thus the uncertainty estimate of the mean of the ensemble of measurements is just the usual standard error of the sample mean. The other Type B uncertainties are absorbed into this estimate. This at first glance may seem like a surprising result, but makes sense on closer reflection. Given sufficient statistics (i.e. enough individual measurements so that n is not too small), the instrumental uncertainty of each individual measurement is not important. These individual instrumental errors combine with the intrinsic stochastic uncertainty to produce an overall variation in measurement that may be well-described by the standard error of the sample mean.

Appendix B Layout of the Data CD

Note that extra additions to the dataset may have been included since the publishing of this document (due to further analysis, comparisons, or other reasons). Thus the listings here should generally be taken as a fairly detailed indication, though not entirely a complete reference of what is contained on the CD.

Root directory listing:

The data CD is broken up into four basic directories.

`docs`
`results`
`scripts`
`data_files`

Listing of `docs`:

Filename	Bytes	Description
`MUST-wt-coanda.ppt`	2741248	Summary of work, Oct 02, presented to Coanda
`MUST-wt-GMU.ppt`	1304064	George Mason University Workshop presentation, July 02
`MUST-wt-TP9-02.ppt`	1942528	Initial results, TP9 meeting, Jan 02
`MUST-wt-UDMWG.ppt`	2379776	Summary of work to Sep 02 at UDMWG meeting
`MUST-wt-wc-TP9.ppt`	4292096	WT and water channel comparisons, Feb 03
`mustcmp1.pdf`	451182	Journal article on wind tunnel, water channel and field trial comparisons
`mustdoc.pdf`	729430	This technical report
`mustres.pdf`	484566	Journal article on detailed results of the MUST wind tunnel experiments
`photos`	4096	Directory containing photos of experiment

Listing of `results`:

This directory contains higher level analysis of the trials, i.e. intercomparison of various configurations and release points, downwind dependence of plume parameters, crosswind profiles of statistics, data analysis programs, and other summaries of the various derived quantities. The results are generally contained in spreadsheets, with some supporting PostScript figures and Microcal Origin projects. The full listing of all files is too long, so just the subdirectories are listed here. Important particular spreadsheets and other files have been explained throughout the body of this report, and the data files are in some sense self-documenting.

Directory	Description
`calibrations`	Spreadsheets detailing calibrations for each day
`conc-stats`	All analysed data of concentration stats and profiles
`correlations`	Autocorrelation functions and integral time scales
`prob-dist`	Fitted probability distribution parameters and plots
`velprofiles`	Inflow wind and turbulence profiles and analysis

Listing of `scripts`:

This directory contains all the FAN analysis scripts and a few small supporting shell scripts and compiled binaries.

Filename	Bytes	Mode	Description
`Summary`	805	rw-	Description of the various script packages
`acorr.cfg`	3396	rw-	Autocorrelation and time scales configuration
`acorr.mac`	28327	rw-	Autocorrelation macro script
`acorr.pan`	3258	rw-	Autocorrelation panel definition
`base.cfg`	3360	rw-	Baseline correction configuration script
`base.mac`	32034	rw-	Baseline correction macro script
`base.pan`	3207	rw-	Baseline correction panel definition
`findphi`	23790	rwx	Binary utility for prob.mac (compiled C++ code)
`flist`	3159	rw-	List of time series data files
`fzlist`	3878	rw-	List of data files with zero runs included
`mkddir`	619	rwx	Small shell script utility for `prob.mac`
`prob.cfg`	3474	rw-	Probability distribution fitting configuration
`prob.mac`	61680	rw-	Probability distribution fitting macro scripts
`prob.pan`	4402	rw-	Probability distribution panel definition
`racorr`	60	rwx	Launcher for autocorrelation and time scales
`rbase`	59	rwx	Launcher for baseline correction
`rprob`	59	rwx	Launcher for probability distribution fitting
`rspec`	59	rwx	Launcher for power spectrum estimation
`rstats`	60	rwx	Launcher for time series statistics extraction
`rview1`	49	rwx	Launcher for real time data processing
`spec.cfg`	3367	rw-	Power spectrum configuration script
`spec.mac`	33383	rw-	Power spectrum estimation macro script
`spec.pan`	3293	rw-	Power spectrum estimation panel definition
`stats.cfg`	3455	rw-	Time series statistics configuration script
`stats.mac`	36478	rw-	Time series statistics macro script
`stats.pan`	2266	rw-	Time series statistics panel definition
`view1.cfg`	3052	rw-	Real time data processing configuration script
`view1.mac`	43175	rw-	Real time data processing macro script
`view1.pan`	5066	rw-	Real time data processing panel definition

Listing of `data_files`:

Due to the great number of files in the subdirectories of the `data_files` directory tree, only the actual trials performed will be listed (and not the many supporting files and results—browse the CD for a full listing). The trials are listed in the order in which they were performed.

Puff data: All puff data is located in the directory `/data_files/npb00ij`. Each individual puff time series comprises a single file, and files are named `npb00ij##.bin`, where `##` ranges over the values 0, 1, 2,..., 60, 61.

Continuous release concentration data:

trial name	u_{50} (ms^{-1})	Q (cm^3/min)	**trial name**	u_{50} (ms^{-1})	Q (cm^3/min)
day1:			day4:		
ncb00ij2	1.74	1646	ncb00ef2	1.81	2939
ncb00ij4	1.75	1646	ncc00ef2	1.83	2939
			ncd00ef2	1.80	2939
day2:			nce00ef2	1.83	2939
ncb00ij5	1.73	1646	ncf00ef2	1.82	2939
ncb00ij1	0.86	1646	ncb33ef2	1.82	4037
ncb00ij3	3.45	1646	ncc33ef2	1.83	4037
ncb00ij6	1.70	2939	ncf33ef2	1.81	4037
ncc00ij2	1.70	2939	ncf49ef2	1.81	4037
ncf00ij2	1.71	2939	ncb49ef2	1.81	4037
ncd00ij2	1.74	2939	ncc49ef2	1.82	4037
nce00ij2	1.71	2939	nca00ve2	1.80	2939
nca00ij2	1.72	2939	ncb00ve2	1.82	2939
day3:			day5:		
nca00gh2	1.82	2939	ncc00ve2	1.81	4037
ncb00gh2	1.82	2939	ncd00ve2	1.81	4037
ncb00gh1	0.92	2939	nce00ve2	1.81	4037
ncb00gh3	3.61	2939	ncf00ve2	1.81	4037
ncb00gh4	1.83	1646	ncb33ve2	1.80	4037
ncc00gh2	1.79	2939	ncc33ve2	1.80	4037
ncd00gh2	1.81	2939	ncf33ve2	1.80	4037
nce00gh2	1.82	2939	ncb49ve2	1.80	4037
ncf00gh2	1.83	2939	ncc49ve2	1.80	4037
ncb33gh2	1.83	2939	ncf49ve2	1.81	4037
ncc33gh2	1.85	2939	ncb00vx2	1.81	2939
ncf33gh2	1.82	2939	ncc00vx2	1.79	2939
ncf49gh2	1.83	2939	ncd00vx2	1.82	2939
ncc49gh2	1.83	2939	ncb00ab2	1.81	5012
ncb49gh2	1.82	2939			
nca00ef2	1.83	2939			

trial name	u_{50} (ms^{-1})	Q (cm^3/min)	**trial name**	u_{50} (ms^{-1})	Q (cm^3/min)
day6:			ncf33ij2	1.80	2939
ncd00ab2	1.80	5012			
ncc00ab2	1.78	5012	stable:		
nca00ab2	1.80	5012	sca00gh1	0.41	2939
nce00ab2	1.80	5012	sca00gh2	0.39	2939
ncf00ab2	1.82	5012	scb00gh1	0.40	2939
ncb33ab2	1.81	5012	scc00gh1	0.40	2939
ncc33ab2	1.80	5012	scf00gh1	0.38	2939
ncf33ab2	1.78	5012	sce00gh1	0.40	2939
ncb49ab2	1.77	5012	scd00gh1	0.38	2939
ncc49ab2	1.80	5012	scd00ij1	0.40	886
ncf49ab2	1.81	5012	scb00ij1	0.40	886
ncf49ij2	1.78	2939	sce00ij1	0.43	886
ncb49ij2	1.82	2939	scc00ij1	0.42	886
ncc49ij2	1.81	2939	sce00ve1	0.36	1646
ncb33ij2	1.81	2939	scc00ve1	0.41	1646
ncc33ij2	1.80	2939			

Velocity time series data files. "Vane" refers to the vane anemometer reading for each time series recorded:

trial name	**vane** (ms^{-1})	**trial name**	**vane** (ms^{-1})	**trial name**	**vane** (ms^{-1})
uwv10050_1	1.06	uwv30050	0.89	uwv50400	1.50
uwv10050_2	1.08	uwv30100	1.23	uwv50600	1.60
uwv10050_3	1.10	uwv30150	1.36	uwv50800	1.65
uwv10100	1.18	uwv30250	1.56	uwv51000	1.78
uwv10150_1	1.11	uwv30400	1.66	uwv60050	0.81
uwv10150_2	1.17	uwv30600	1.71	uwv60100	1.19
uwv10250	1.27	uwv30800	1.85	uwv60150	1.32
uwv10400	1.33	uwv31000	1.92	uwv60250	1.44
uwv10600	1.48	uwv40050	0.96	uwv60400	1.53
uwv10800	1.58	uwv40100	1.13	uwv60600	1.56
uwv11000_1	1.61	uwv40150	1.24	uwv60800	1.70
uwv11000_2	3.30	uwv40250	1.39	uwv61000	1.81
uwv11000_3	0.87	uwv40400	1.50	uvv60050	0.81
uwv20050	0.87	uwv40600	1.60	uvv60100	1.19
uwv20100	1.21	uwv40800	1.73	uvv60150	1.32
uwv20150	1.36	uwv41000	1.74	uvv60250	1.44
uwv20250	1.51	uwv50050	0.88	uvv60400	1.53
uwv20400	1.60	uwv50100	1.14	uvv60600	1.56
uwv20600	1.77	uwv50150	1.28	uvv60800	1.70
uwv20800	1.79	uwv50250	1.37	uvv61000	1.81
uwv21000	1.85				

DISTRIBUTION LIST

Wind Tunnel Simulations of the Mock Urban Setting Test—Experimental Procedures and Data Analysis

Ralph Gailis

	Number of Copies
DEFENCE ORGANISATION	
Task Sponsor	
Land Development - LtCol Damon Howes	1
S&T Program	
Chief Defence Scientist FAS Science Policy AS Science Corporate Management Director General Science Policy Development	1
Counsellor, Defence Science, London	Doc Data Sheet
Counsellor, Defence Science, Washington	Doc Data Sheet
Scientific Adviser to MRDC, Thailand	Doc Data Sheet
Scientific Adviser Joint	1
Navy Scientific Adviser	Doc Data Sheet and Dist List
Scientific Adviser, Army	1
Air Force Scientific Adviser	Doc Data Sheet and Dist List
Scientific Adviser to the DMO M&A	Doc Data Sheet and Dist List
Scientific Adviser to the DMO ELL	Doc Data Sheet and Dist List
Platform Sciences Laboratory	
Head CBRN Defence Centre - Dr. Simon Oldfield	1
Hazard Managment Functional Area Leader - Dr. Ralph Leslie	1
Task Manager - Mr. Errol O'Donovan	1
Author - Dr. Ralph Gailis	1
DSTO Library and Archives	
Library Fishermans Bend	Doc Data Sheet
Library Edinburgh	1
Defence Archives	1
Capability Systems Staff	
Director General Maritime Development	Doc Data Sheet
Director General Land Development	1

Director General Information Capability Development	Doc Data Sheet
Office of the Chief Information Officer	
Deputy CIO	Doc Data Sheet
Director General Information Policy and Plans	Doc Data Sheet
AS Information Strategies and Futures	Doc Data Sheet
AS Information Architecture and Management	Doc Data Sheet
Director General Australian Defence Simulation Office	Doc Data Sheet
Strategy Group	
Director General Military Strategy	Doc Data Sheet
Director General Preparedness	Doc Data Sheet
HQAST	
SO (Science) (ASJIC)	Doc Data Sheet
Navy	
Director General Navy Capability, Performance and Plans, Navy Headquarters	Doc Data Sheet
Director General Navy Strategic Policy and Futures, Navy Headquarters	Doc Data Sheet
Air Force	
SO (Science), Headquarters Air Combat Group, RAAF Base, Williamstown NSW 2314	Doc Data Sheet and Exec Summ
Army	
ABCA National Standardisation Officer, Land Warfare Development Sector, Puckapunyal	Doc Data Sheet
SO (Science), Land Headquarters (LHQ), Victoria Barracks, NSW	Doc Data Sheet and Exec Summ
SO (Science), Deployable Joint Force Headquarters (DJFHQ)(L), Enoggera, Queensland	Doc Data Sheet
NPOC QWG Engineer NBCD Combat Development Wing, Puckapunyal,Vic	1
Intelligence Program	
DGSTA, Defence Intelligence Organisation	1
Manager, Information Centre, Defence Intelligence Organisation	1 (pdf format)
Assistant Secretary Corporate, Defence Imagery and Geospatial Organisation	Doc Data Sheet
Defence Materiel Organisation	
Deputy CEO	Doc Data Sheet
Head Aerospace Systems Division	Doc Data Sheet
Head Maritime Systems Division	Doc Data Sheet

Chief Joint Logistics Command	Doc Data Sheet
Head Materiel Finance	Doc Data Sheet
Defence Libraries	
Library Manager, DLS-Canberra	Doc Data Sheet
Library Manager, DLS-Sydney West	Doc Data Sheet
UNIVERSITIES AND COLLEGES	
Australian Defence Force Academy Library	1
Head of Aerospace and Mechanical Engineering, ADFA	1
Deakin University Library, Serials Section (M List), Geelong, Vic	1
Hargrave Library, Monash University	Doc Data Sheet
Librarian, Flinders University	1
OTHER ORGANISATIONS	
National Library of Australia	1
NASA (Canberra)	1
INTERNATIONAL DEFENCE INFORMATION CENTRES	
US Defense Technical Information Center	2
UK Defence Research Information Centre	2
Canada Defence Scientific Information Service	1
NZ Defence Information Centre	1
ABSTRACTING AND INFORMATION ORGANISATIONS	
Library, Chemical Abstracts Reference Service	1
Engineering Societies Library, US	1
Materials Information, Cambridge Scientific Abstracts, US	1
Documents Librarian, The Center for Research Libraries, US	1
SPARES	
DSTO Edinburgh Library	5
Total number of copies:	35

DEFENCE SCIENCE AND TECHNOLOGY ORGANISATION DOCUMENT CONTROL DATA				1. CAVEAT/PRIVACY MARKING
2. TITLE Wind Tunnel Simulations of the Mock Urban Setting Test—Experimental Procedures and Data Analysis			3. SECURITY CLASSIFICATION Document (U) Title (U) Abstract (U)	
4. AUTHOR Ralph Gailis			5. CORPORATE AUTHOR Platforms Sciences Laboratory 506 Lorimer St, Fishermans Bend, Victoria, Australia 3207	
6a. DSTO NUMBER DSTO–TR–1532	6b. AR NUMBER 013–153		6c. TYPE OF REPORT Technical Report	7. DOCUMENT DATE July, 2004
8. FILE NUMBER 2003/75439/1	9. TASK NUMBER ARM 02/085	10. SPONSOR DGLD	11. No OF PAGES 47	12. No OF REFS 26
13. URL OF ELECTRONIC VERSION http://www.dsto.defence.gov.au/corporate/reports/DSTO–TR–1532.pdf			14. RELEASE AUTHORITY Director, Platforms Sciences Laboratory	

15. SECONDARY RELEASE STATEMENT OF THIS DOCUMENT

Approved For Public Release

OVERSEAS ENQUIRIES OUTSIDE STATED LIMITATIONS SHOULD BE REFERRED THROUGH DOCUMENT EXCHANGE, PO BOX 1500, EDINBURGH, SOUTH AUSTRALIA 5111

16. DELIBERATE ANNOUNCEMENT

No Limitations

17. CITATION IN OTHER DOCUMENTS

No Limitations

18. DEFTEST DESCRIPTORS

Wind tunnel tests
Field tests
Urban defence
Atmospheric diffusion
Boundary layer flow
Contaminants

19. ABSTRACT

The MUST experiment was a large outdoor field study in atmospheric dispersion, attempting to simulate an urban boundary layer by the construction of a regular array of shipping containers. The current report gives details of a wind tunnel dispersion study of the MUST array, aimed at bridging some of the gaps between laboratory and full-scale outdoor trials. The experimental setup and wind tunnel instrumentation are discussed in detail, the measurements made together with the organisation of the dataset is fully described, and a comprehensive description of the data analysis techniques is given. Emphasis is placed on the scaling arguments used to compare data between a wind tunnel and full-scale study, and on methods of uncertainty analysis to provide a rigorous underpinning to the dataset. The report serves as a complete documentation for users of the MUST wind tunnel simulation dataset, which can be obtained by contacting the author.